Appendix A. Further Discussion and Results of the Shorted Turn Fault Test

A.1. Current Harmonics Induced in the Rotor Winding

The air-gap MMF which is produced by the stator winding of a squirrel cage three-phase 2p-pole induction motor can be expressed as in (Eq. A.1), assuming that the three-phase supply is balanced [19].

$$F_s(t,x) = \frac{3N_s I_s}{\pi} \sum_{v_s=1}^{\infty} \left\{ \frac{1}{v_s} \left[\sum_{b=1}^{c} sin\left(v_s \frac{\tau_{cb}}{\tau_p} \frac{\pi}{2} \right) \right] \times sin\left(\omega_s t \pm \frac{v_s \pi}{\tau_p} x \right) \right\} \quad \text{(Eq. A.1)}$$

where v_s is the stator MMF space harmonic rank, I_s is the maximum value of the stator phase current, ω_s is the angular supply frequency, N_s is the number of turns of each stator coil, c is the number of coils of each stator phase, τ_{cb} is the b^{th} coil pitch, τ_p is the pole step, and x is the circumferential angular position.

This stator MMF in the air-gap causes a flux to be induced in the rotor. The flux induced in the α^{th} mesh of the rotor is given by (Eq. A.2) [19].

$$\Phi_{sr,\alpha}(t) = \int_{x_1}^{x_2} \frac{\mu_0 F_s(t,x)}{\delta} l_c \, dx \qquad \text{(Eq. A.2)}$$

where μ_o is the magnetic permeability of air, l_c is the core length, δ is the air gap length, and x_1, x_2 are the defined angular positions of the α^{th} mesh.

Hence,

$$\Phi_{sr,\alpha}(t) = \sum_{v_s=1}^{\infty} \Phi_{max\, v_s} sin\Bigg([1 \pm v_s(1-s)] \times \omega_s t \pm \frac{2v_s\pi(k-1)}{pR} \Bigg) \qquad \text{(Eq. A.3)}$$

where

$$\Phi_{max\, v_s} = \frac{3\mu_0 N_s I_s l_c D_r}{p^2 \pi \delta} \sum_{b=1}^{c} sin\left(v_s \frac{\tau_{cb}}{\tau_p} \frac{\pi}{2} \right) \times sin\left(v_s p \frac{\pi}{R} \right) \qquad \text{(Eq. A.4)}$$

and D_r is the external rotor diameter.

The presence of shorted turn faults in the stator windings will affect the distribution of the stator MMF in the air-gap because a degree of the stator current will now flow through the short-circuited turns. Therefore by considering the relationship of the induced flux in (Eq. A.3) and the affected stator MMF, the presence of shorted turn faults will be expected to introduce new frequency components (Eq. A.5) in the rotor currents [19, 36]. A generalisation of these fault frequency components which include the stator time harmonics is shown in (Eq. 5.1).

$$f_{rotor\, st} = f\left[k\frac{1-s}{p} \pm 1 \right] \qquad \text{(Eq. A.5)}$$

where $k = 1, 2, 3, \ldots$

A.2. Current Harmonics Induced in the Stator Winding

The air-gap MMF which is produced by the rotor winding is shown in (Eq. A.6) [19].

$$F_r(t,x) = \sum_{v_r=1}^{\infty} \frac{RI_{rv\,max}}{\pi} \sum_{k=1}^{\infty} \frac{1}{k} sin\left(\frac{k\tau_{cr}}{2}\right) \times sin\,(kRx \pm s\omega_s t) \qquad \text{(Eq. A.6)}$$

where $I_{rv\ max}$ is the maximum value of the v_r^{th} harmonic rotor current and τ_{cr} is the rotor equivalent coil pitch.

This rotor MMF in the air-gap causes a flux to be induced in the stator winding. The final expression of the flux induced by the k^{th} harmonics in the b^{th} stator coil is given in (Eq. A.7) [19].

$$\Phi_{rs,b,k}(t) = \Phi_{max\,b,k} sin\left[kR\frac{\omega_r}{p}t \pm v\omega_s t + k\frac{2\pi(b-1)}{3}\right] \qquad \text{(Eq. A.7)}$$

where ω_r is the angular rotor frequency and

$$\Phi_{max\,b,k} = \frac{\mu_0 I_{rv\,max} R l_c D_r N_s}{\pi\delta k^2} sin\left(\frac{k\tau_{cr}}{2}\right) sin\left(k\frac{\pi}{2}\frac{\tau_{cb}}{\tau_p}\right) \qquad \text{(Eq. A.8)}$$

The presence of shorted turn faults in the stator windings is expected to affect the frequency components that exist in the stator current. By considering the induced flux relation in (Eq. A.7), the shorted turn faults will be expected to vary the frequency components in (Eq. A.9) in the stator current [19, 37]. A generalisation of these fault frequency components is the frequency components in (Eq. 5.3).

$$f_{stator\ st} = f\left[kR\frac{1-s}{p} \pm v\right] \qquad \text{(Eq. A.9)}$$

A.3. Experimental Results for Turn to Turn Fault Analysis Using Fundamental Sidebands of Rotor Frequency Harmonics

Components at $k = 2$ and $v = \pm 1$

Figure A.1 shows how the frequency components in (Eq. 5.1) at $k = 2$ and $v = \pm 1$ in the current and the leakage flux signals vary under different loading and turn to turn conditions. The figure shows that both the upper ($v = +1$) and the lower ($v = -1$) sidebands in the current and the flux signals do not display consistent and significant magnitude variation between the different turn to turn severities. As a consequence, these frequency components may not be suitable for turn to turn features.

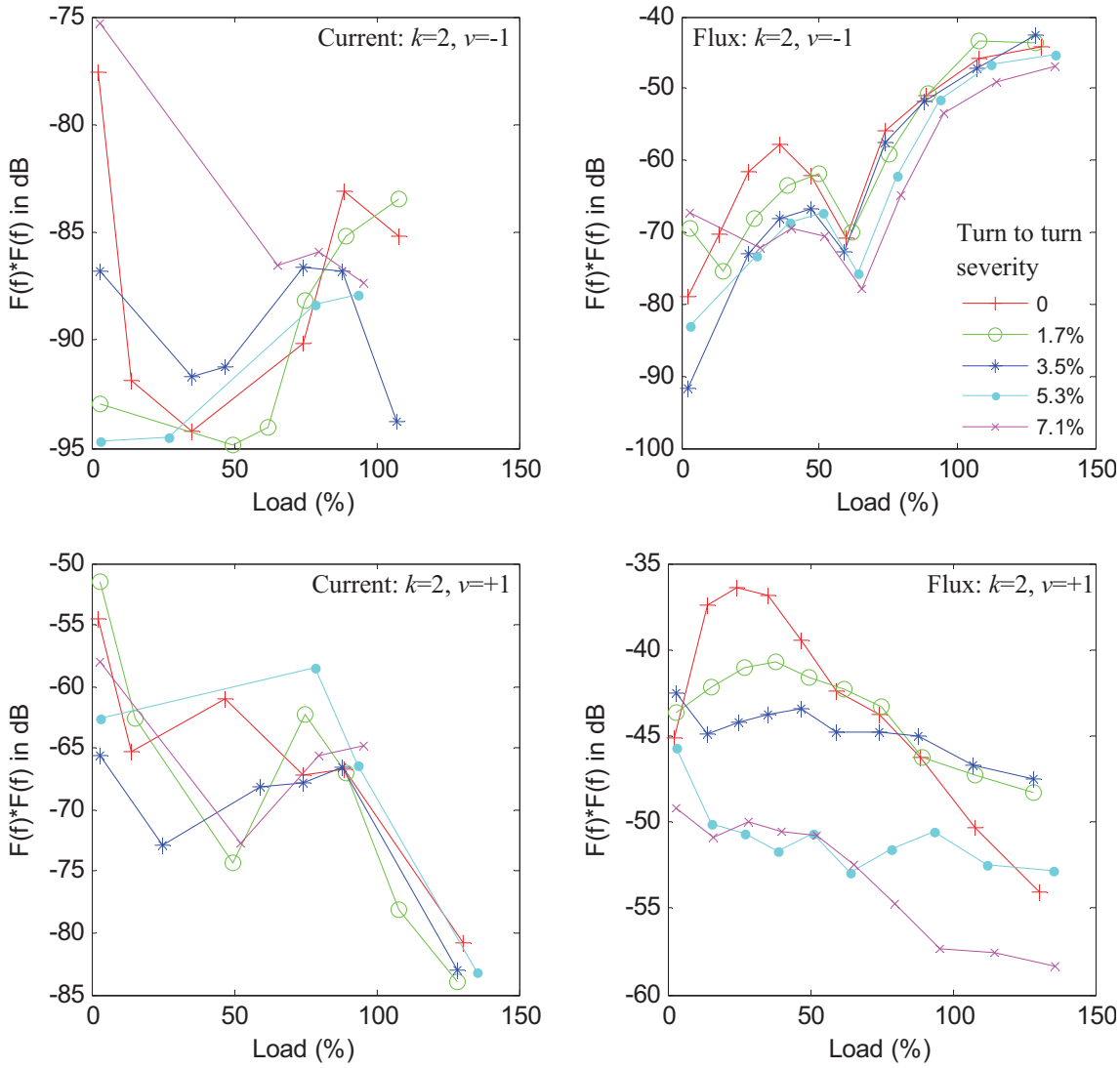

Figure A.1 – Magnitude of the frequency components in (Eq. 5.1) at $k = 2$ and $v = \pm 1$ in the current and the leakage flux signals as a function of load.

Components at $k = 3$ and $v = \pm 1$

Figure A.2 shows that these frequency components cannot be considered as turn to turn features because they may have low signal to noise ratio (hence difficult to detect) and they do not show significant and consistent magnitude variation between the healthy and the faulty conditions.

Based on the analysis so far, it seems that the effectiveness of the frequency components in (Eq. 5.1) to detect turn to turn faults reduces as the variable k is increased. As the variable k is increased, the magnitude of the frequency components in (Eq. 5.1) seems to get weaker and weaker. Therefore, it is desirable to keep the variable k in (Eq.

5.1) to 1, which is the value that the shorted turn investigation in this thesis will concentrate on.

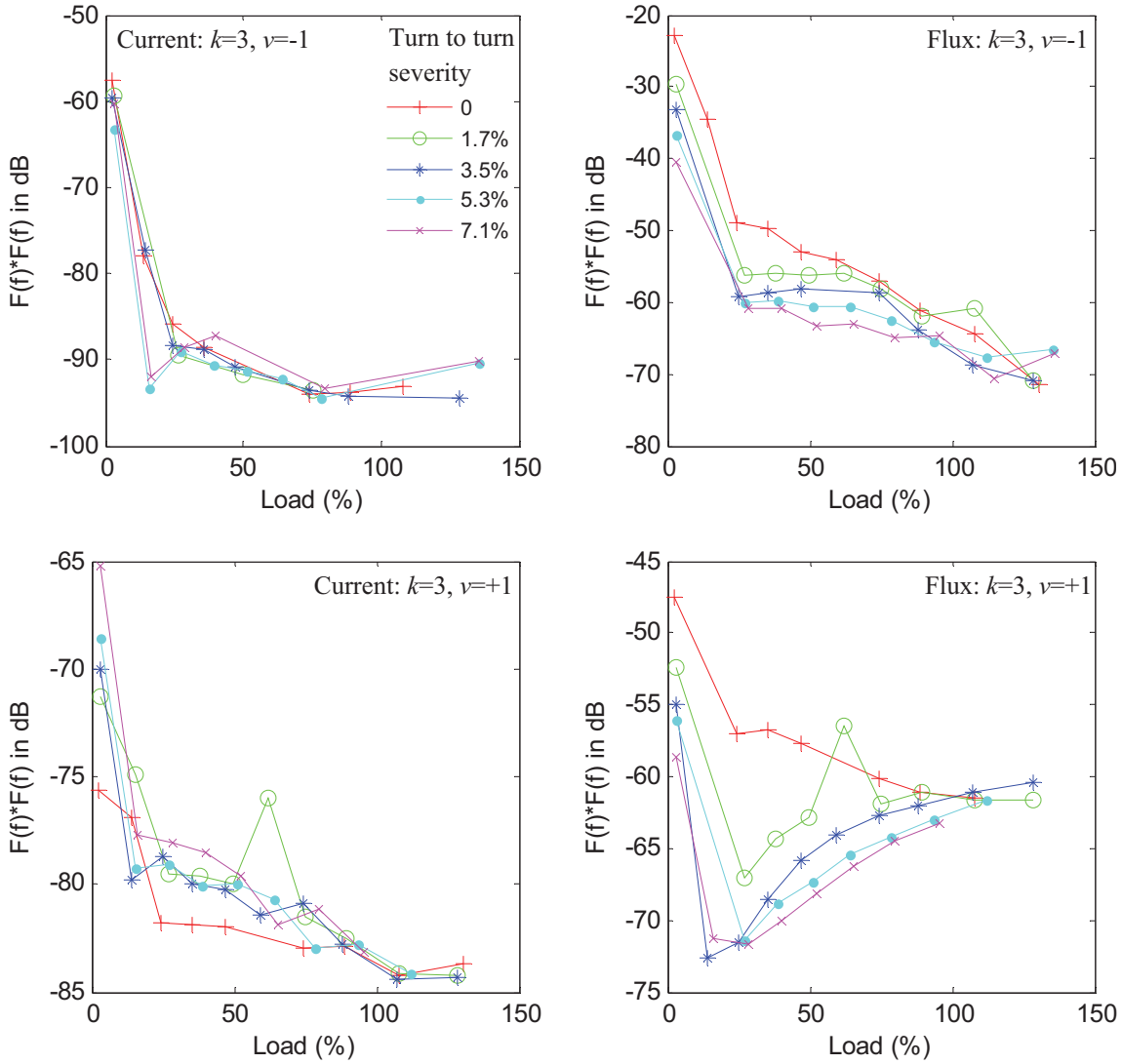

Figure A.2 – Magnitude of the frequency components in (Eq. 5.1) at $k = 3$ and $v = \pm 1$ in the current and the leakage flux signals as a function of load.

Components at $k = 1$ and $v = \pm 3$

Figure A.3 shows that the frequency components in the current signal mostly show no significant magnitude variation (i.e. less than 5 dB) among the different fault severities. On the other hand, the frequency components in the flux signal show significant magnitude variation between the healthy and the faulty motors (i.e. about 5 - 15 dB difference between the healthy and the 7.1% fault), where the magnitude consistently decreases as the

severity of the fault increases. Therefore, the frequency components in the flux signal can be considered as turn to turn features.

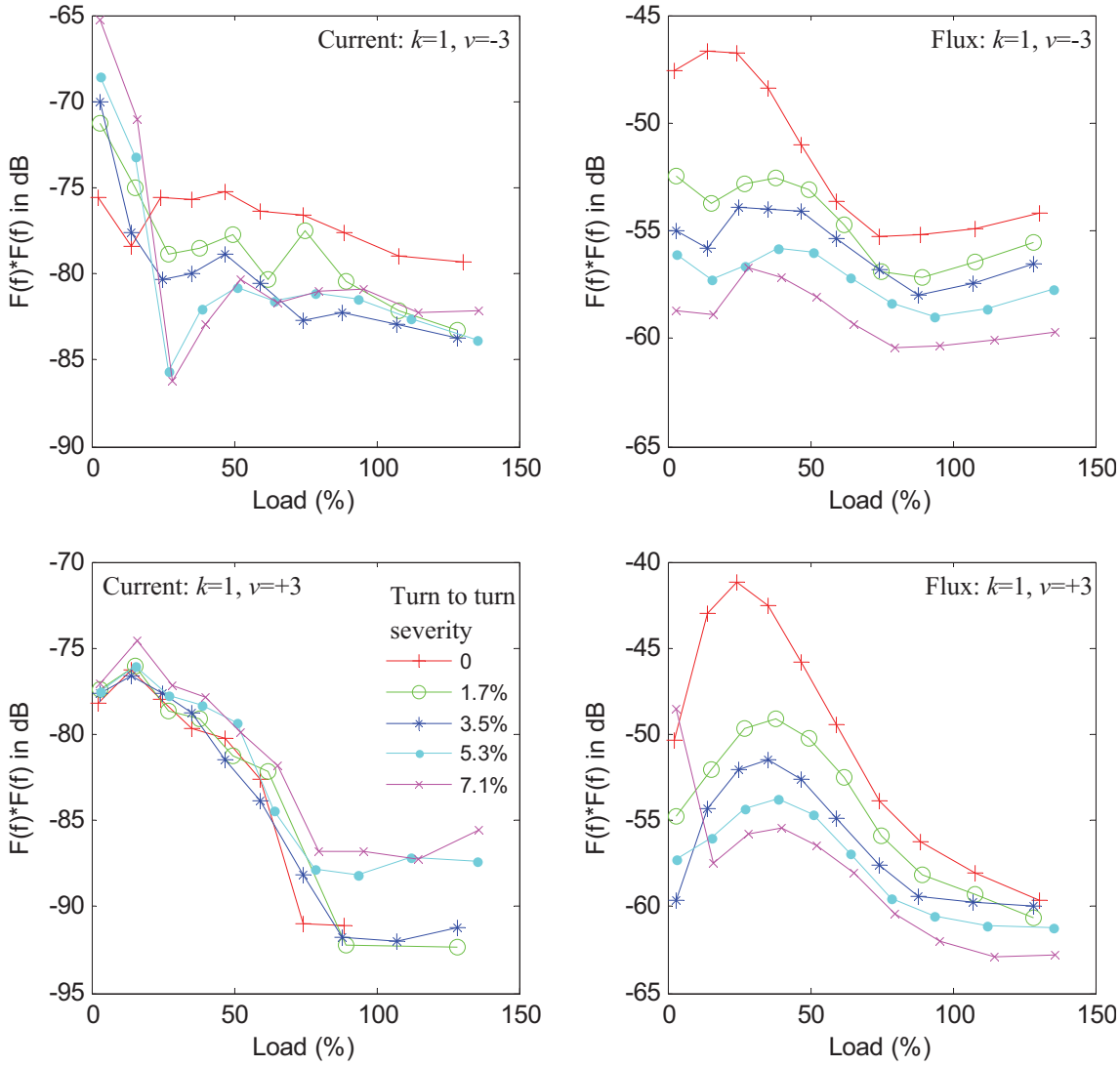

Figure A.3 - Magnitude of the frequency components in (Eq. 5.1) at $k = 1$ and $v = \pm 3$ from the current and leakage flux signals as a function of load.

Components at $k = 1$ and $v = \pm 5$

Figure A.4 shows that the frequency components in the current signal cannot be considered as features because they have low signal to noise ratio and their magnitude variation between the different fault severities is not significant and not consistent.

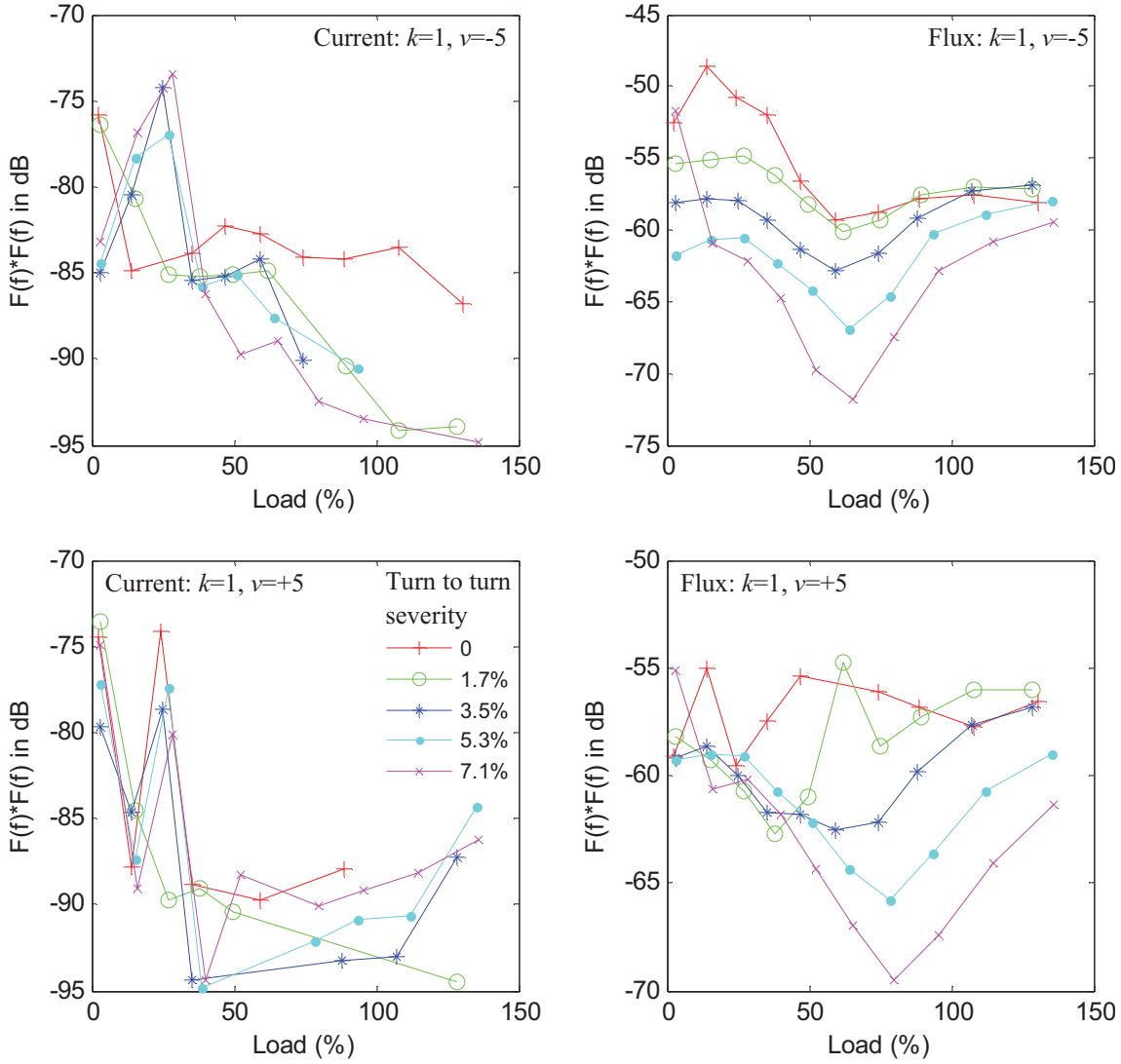

Figure A.4 - Magnitude of the frequency components in (Eq. 5.1) at $k = 1$ and $v = \pm 5$ from the current and the leakage flux signals as a function of load.

Similarly, the upper sideband in the leakage flux signal does not show consistent magnitude variation between the different fault severities but it can distinguish the healthy and certain faulty (i.e. greater than 5.3%) conditions when the load is greater than 60%. The magnitude of this sideband is generally found to be weaker (by about 5 – 10 dB) than the magnitude of the component counterparts at $v = +1$ and $+3$. On the other hand, the lower sideband in the flux signal shows a more consistent magnitude variation between the different fault severities, where the magnitude tends to decrease as the severity of the fault increases. However, the magnitude variation is found to be smaller and less consistent than the magnitude variation of the flux components at $v = -1$ and $v = -3$.

A.4. Experimental Results for Turn to Turn Fault Analysis Using Twice Supply Frequency

Figure A.5 - Figure A.7 show how the magnitudes of the twice supply frequency component in the vibration sensor signals vary under the different loading and turn to turn fault conditions. Figure A.5 shows that the frequency component from the DEH vibration signal can only distinguish between the healthy and the 7.1% fault (20 shorted turns) effectively, where the magnitude of the healthy condition is about 5 dB lower than the magnitude of the faulty condition. Similarly the frequency component from the NDEH vibration signal (Figure A.6) can distinguish between the healthy and only the 7.1% fault condition when the load is less than 60% but when the load is greater than 60%, the component can distinguish the healthy, 5.3% fault, and 7.1% fault conditions. On the other hand, the twice supply frequency component in the DEV vibration signal (Figure A.7) does not show observable magnitude variation among the different fault severities, except at the no load condition. Hence, it cannot be considered to be a useful feature.

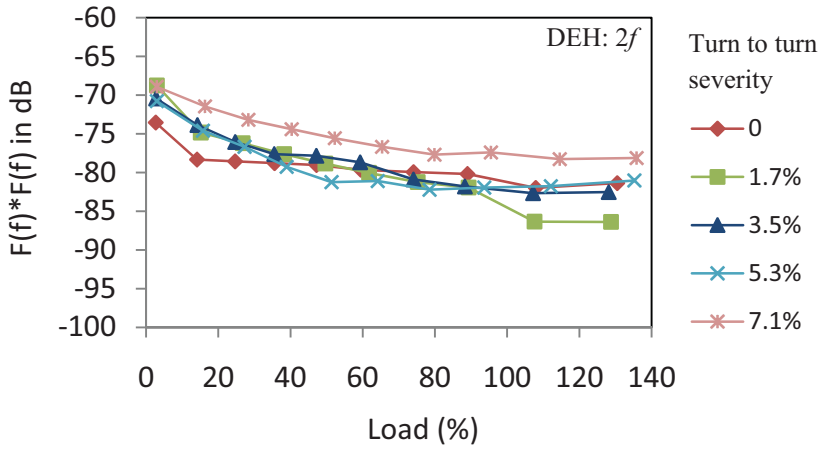

Figure A.5 – Magnitude of the twice supply frequency in the DEH vibration signal as a function of load.

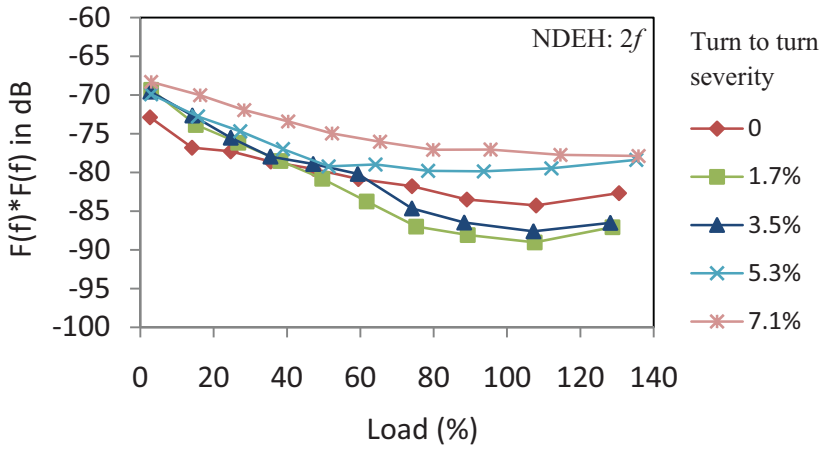

Figure A.6 - Magnitude of the twice supply frequency in the NDEH vibration signal as a function of load.

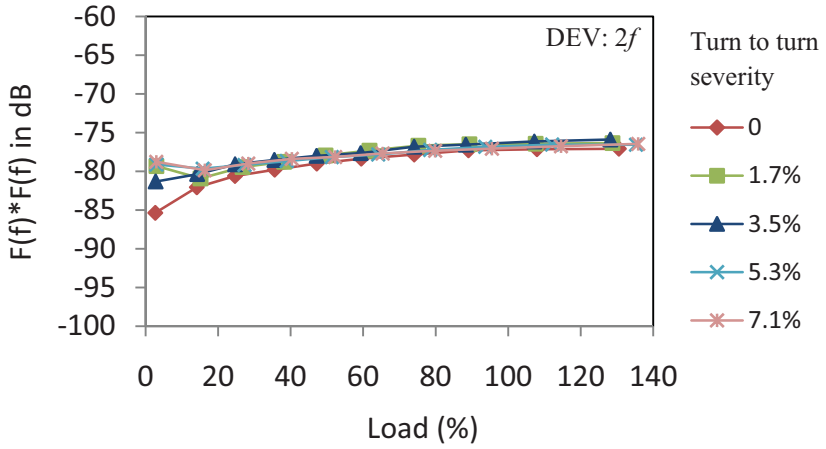

Figure A.7 - Magnitude of the twice supply frequency in the DEV vibration signal as a function of load.

A.5. Experimental Results for Turn to Turn Fault Analysis Using Rotor Slot Harmonics

Components at $n_d = 0$, $k = 1$, and $v = \pm 1$

Figure A.8 shows how the magnitude of the frequency components varies under the different loading conditions and the different turn to turn fault severities. The figure shows that the lower sideband component in the current signal can distinguish between the healthy, 5.3% fault, and 7.1% fault conditions, where the magnitude tends to increase as the severity of the fault increases, although the magnitude variation is not great (about 5 dB between the healthy and the 7.1% fault). As a result, this frequency component may only

be used as a feature to detect turn to turn faults if the fault severity is greater than or equal to 5.3%. On the other hand, the upper sideband component in the current signal shows no useful magnitude variation among the different fault severities.

Figure A.8 also demonstrates that the frequency components in the flux signal show some magnitude variation between the healthy and the faulty conditions (about 5 to 10 dB between the healthy and the 7.1% fault). However, the magnitude variations are not consistent enough for these frequency components to be considered as good turn to turn features.

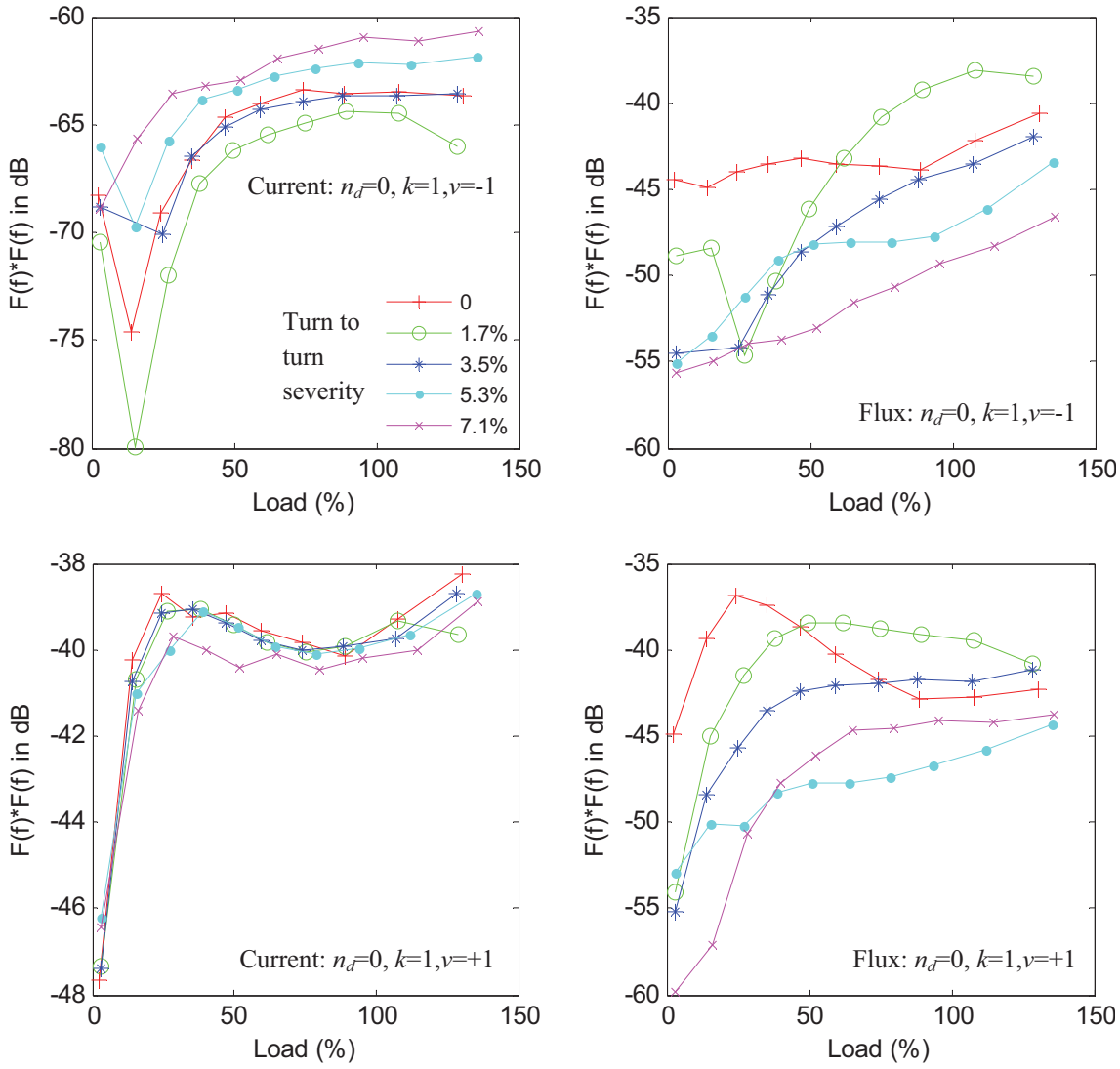

Figure A.8 - Magnitude of the frequency components in (Eq. 5.3) at $n_d = 0$, $k = 1$, $v = -1$ (top), $n_d = 0$, $k = 1$, $v = +1$ (bottom), from the current and leakage flux signals as a function of load.

Components at $n_d = 0$, $k = 2$, and $v = \pm 1$

Figure A.9 shows the magnitude variations of the rotor slot harmonics (at $n_d = 0$, $k = 2$, and $v = \pm 1$) from the current and the leakage flux signals under different loading and turn to turn conditions. The figure shows that the magnitude of these components are weaker (by about 45 dB in the current signal and about 15 dB in the flux signal) than the counterpart components at $k = 1$. Unlike the components at $k = 1$ in the flux signal, the magnitude of these frequency components in both current and flux signals do not show any consistent variation among the different fault severities.

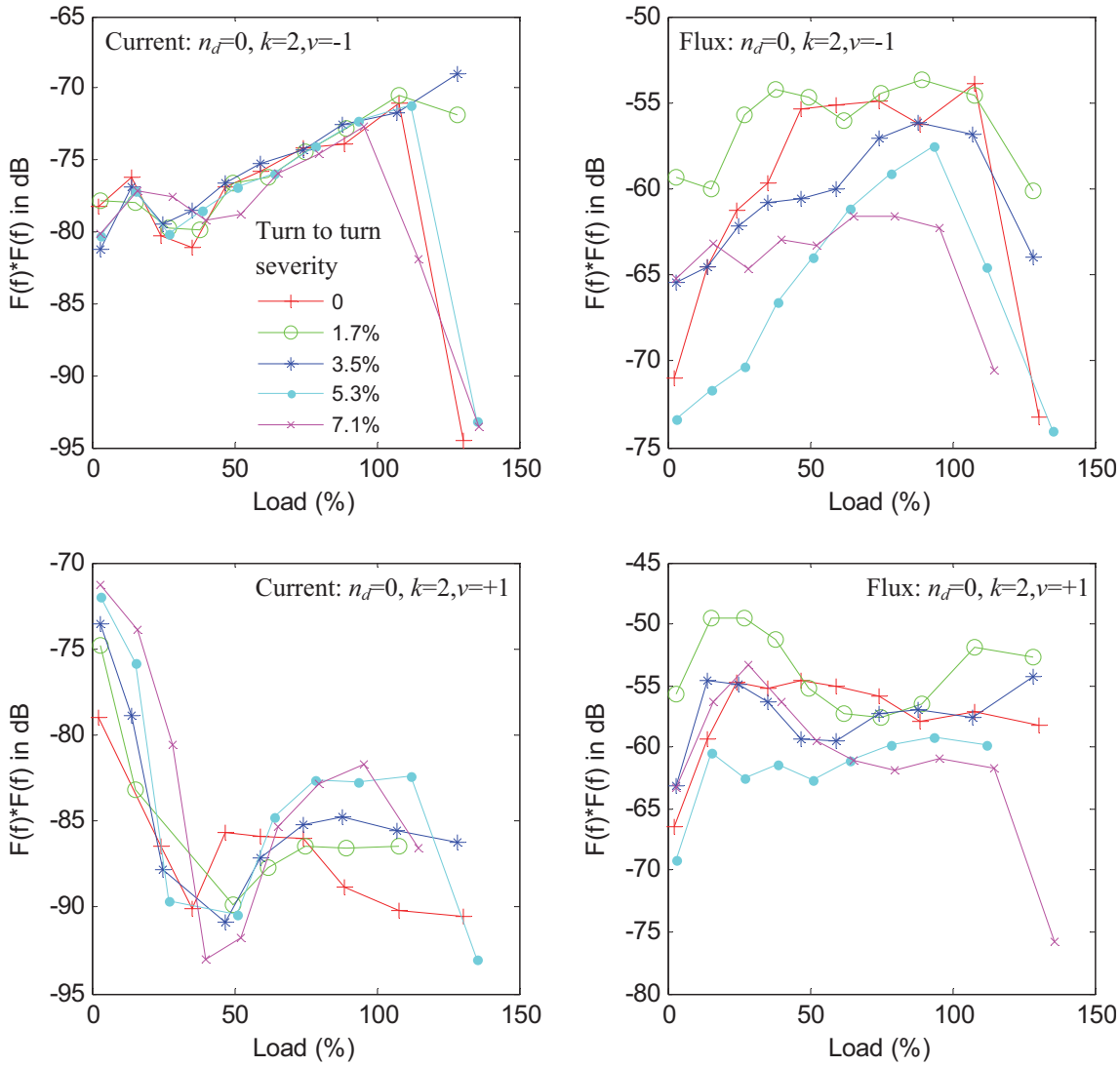

Figure A.9 - Magnitude of the frequency components in (Eq. 5.3) at $n_d = 0$, $k = 2$ and $v = \pm 1$ from the current and leakage flux signals as a function of load.

Components at $n_d = 0$, $k = 3$, and $v = \pm 1$

Figure A.10 shows that the magnitudes of the sidebands in the current signal fluctuate between -90 and -95 dB under the different loading and turn to turn conditions. These magnitudes are weaker than the counterpart components at $k = 1$ and $k = 2$, and they can be difficult to detect. In addition, the magnitude variations among the different fault severities show no useful pattern.

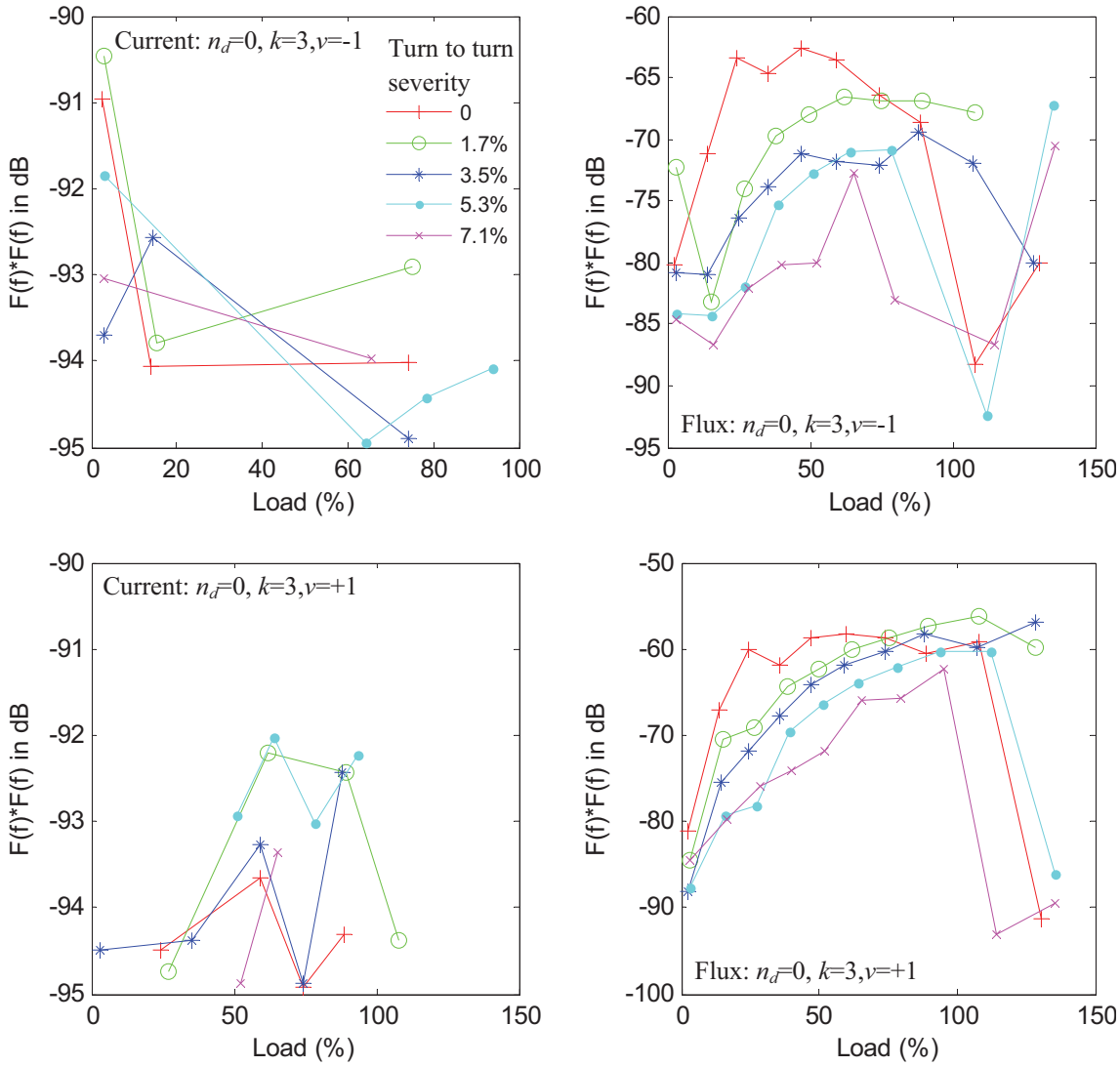

Figure A.10 - Magnitude of the frequency components in (Eq. 5.3) at $n_d = 0$, $k = 3$ and $v = \pm 1$ from the current and leakage flux signals as a function of load.

Similarly, the magnitudes of the sidebands from the leakage flux signal, which vary between -60 dB and -95 dB, are also weaker than the counterpart components at $k = 1$ and

k = 2. The magnitudes tend to decrease as the severity of the fault increases. However, the magnitude variations among the different fault severities are not better than the counterpart components at k = 1 and they are not consistent enough for these sidebands to be considered as turn to turn features.

Examining the behaviour of the frequency components in (Eq. 5.3) so far, it seems that the magnitude of the frequency components decreases as the variable k increases. This reduction in the magnitude also reduces the effectiveness of the frequency components to detect turn to turn faults. Therefore, it is desirable to keep the variable k to 1, which is the value that the shorted turn investigation in this thesis will concentrate on.

Components at n_d = 0, k = 1, and v = ±3

Figure A.11 shows that the magnitudes of the sidebands in the current signal vary between -45 and -75 dB under the different loading and turn to turn conditions. These magnitudes are weaker than the counterpart components at k = 1 and v = ±1. Although the magnitudes tend to decrease as the fault severity increases, the magnitude variations among the different fault severities are not significant enough (i.e. less than 5 dB). As a consequence, it is difficult to consider these sidebands as turn to turn features.

On the other hand, the sidebands in the leakage flux signal show significant magnitude variation between the healthy and the faulty conditions (i.e. greater than 5 dB), where the magnitude tends to decrease as the severity of the fault increases, especially when the load is less than 80%. However, the magnitudes of these sidebands may not always be able to distinguish the different fault severities.

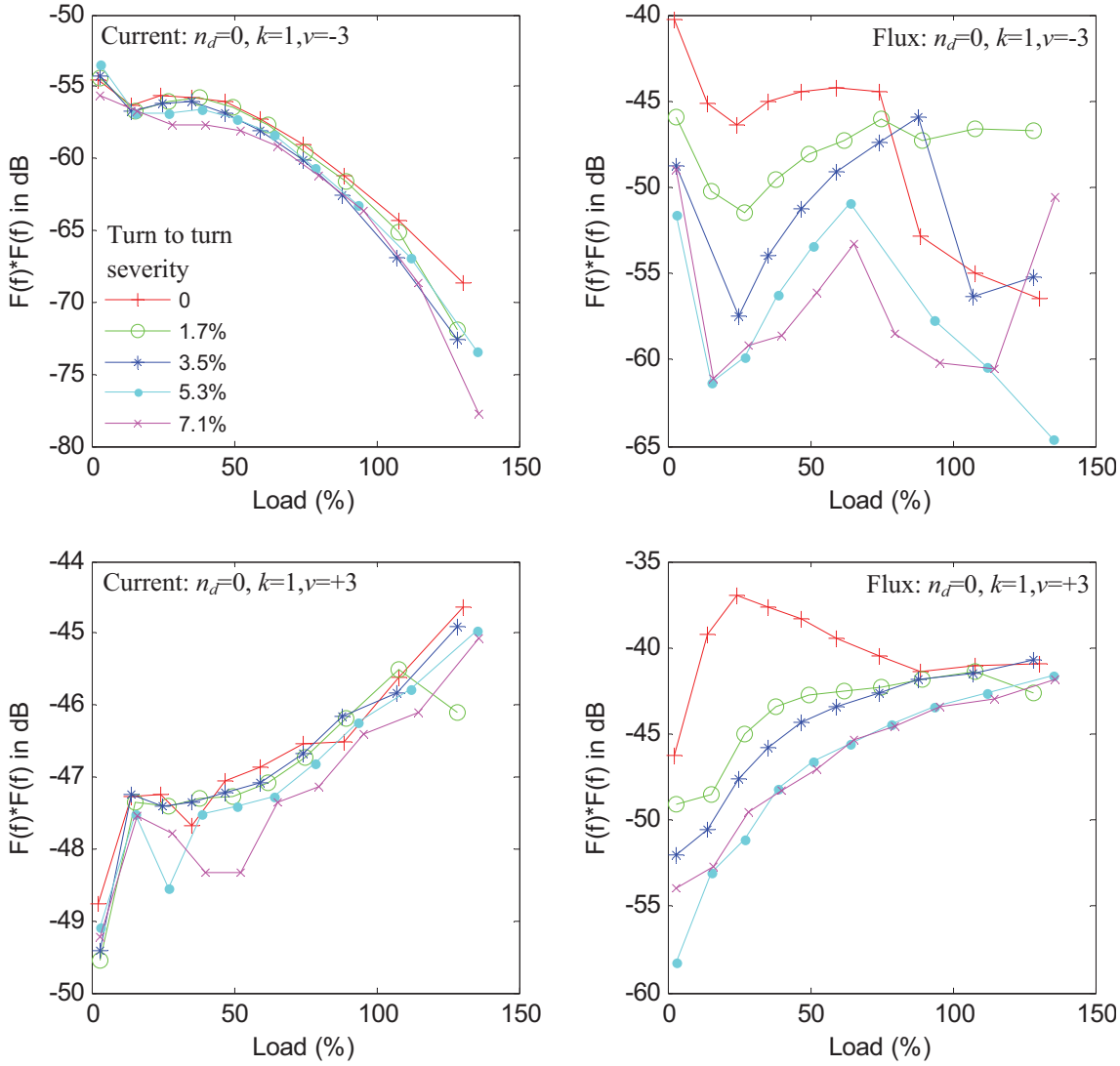

Figure A.11 - Magnitude of the frequency components in (Eq. 5.3) at $n_d = 0$, $k = 1$ and $v = \pm 3$ from the current and leakage flux signals as a function of load.

Components at $n_d = 0$, $k = 1$, and $v = \pm 5$

Figure A.12 shows that the lower sidebands in both current and flux signals cannot be considered as turn to turn features because they do not show significant and consistent magnitude variation (i.e. less than 5 dB) between the healthy and the faulty conditions.

On the other hand, the upper sidebands in both current and flux signals may be used to distinguish between the healthy and some faulty conditions but not to separate the different fault severities. The current sideband shows about 5 - 10 dB increase between the healthy and the 7.1% fault, while the flux sideband shows about 5 - 10 dB decrease between the healthy and the 7.1% fault.

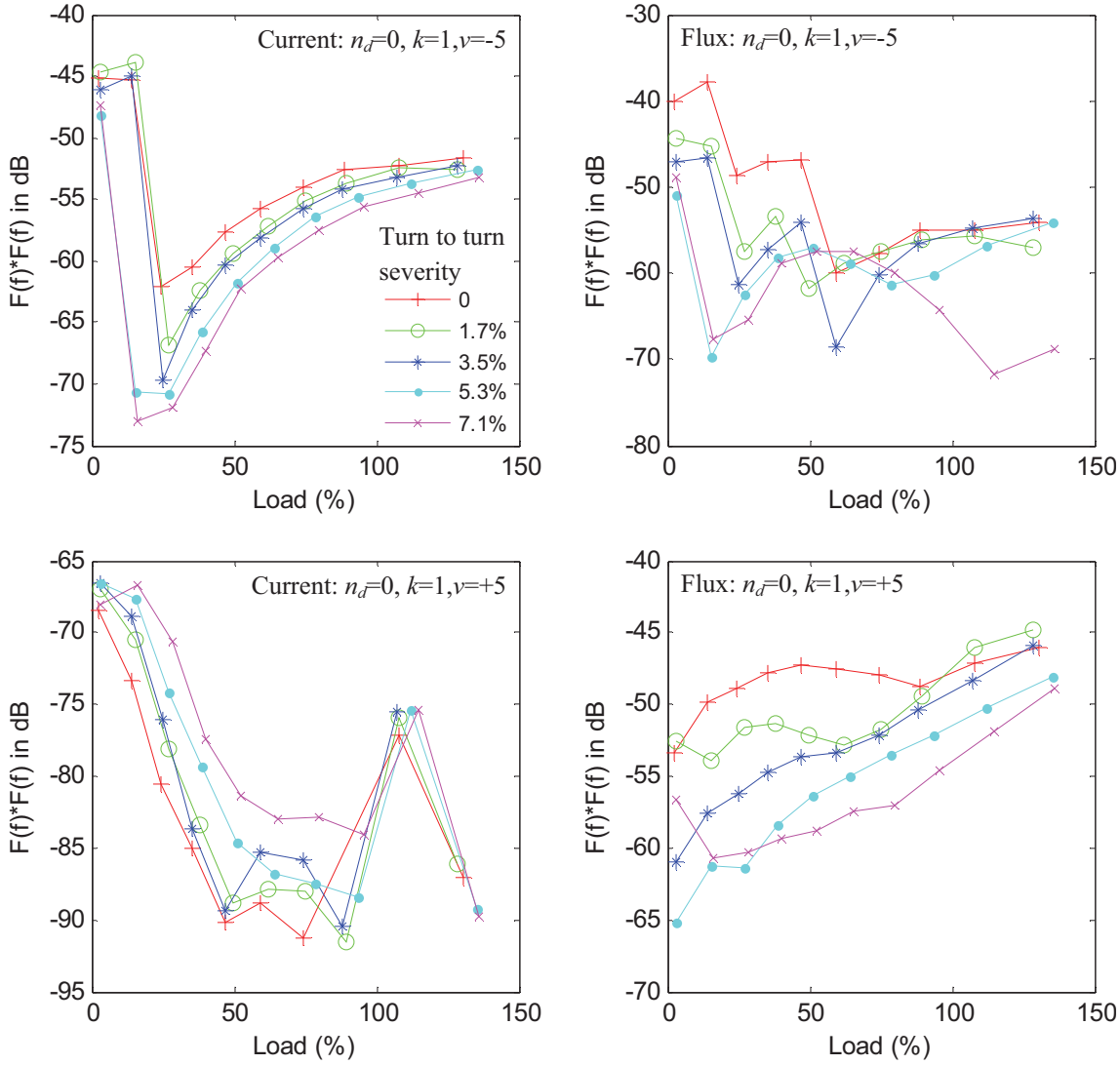

Figure A.12 - Magnitude of the frequency components in (Eq. 5.3) at $n_d = 0$, $k = 1$ and $v = \pm 5$ from the current and leakage flux signals as a function of load.

A.6. Experimental Results for Turn to Turn Fault Analysis Using Third Harmonic of the Fundamental

Figure A.13 and Figure A.14 show how the magnitude of the frequency component at $3f$ in the stator current and the axial leakage flux signals varies under different loading conditions and different turn to turn fault severities.

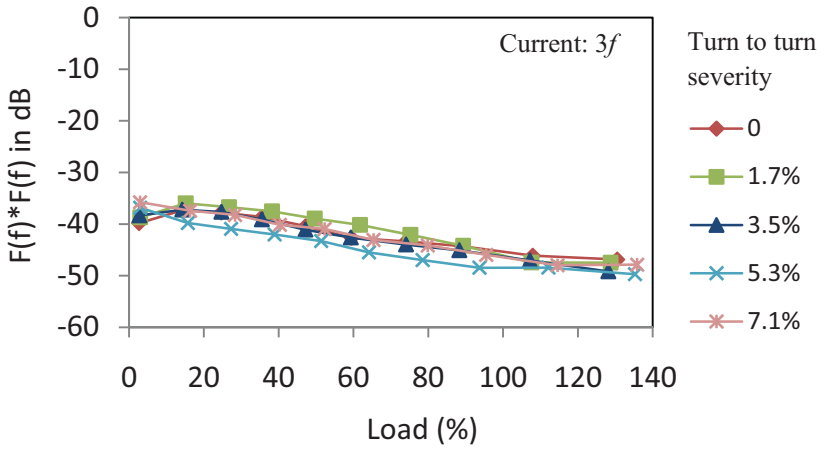

Figure A.13 – Magnitude of the third fundamental harmonic in the current signal as a function of load.

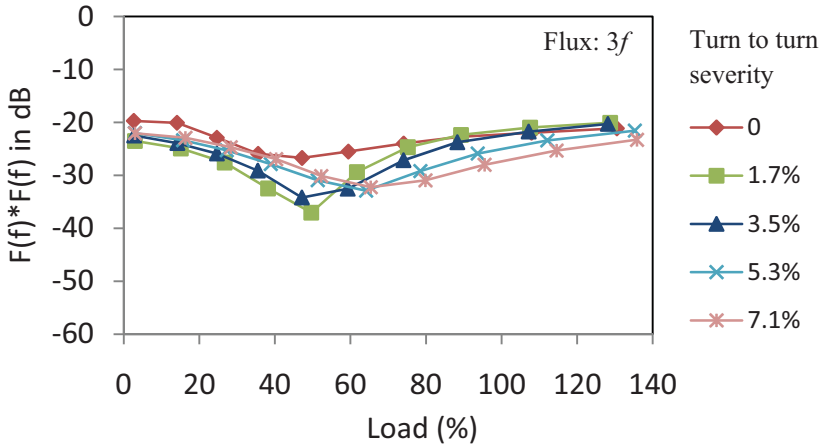

Figure A.14 - Magnitude of the third fundamental harmonic in the leakage flux signal as a function of load.

A.7. Experimental Results for Phase to Phase Turn Fault Analysis Using Fundamental Sidebands of Rotor Frequency Harmonics

Figure A.15 show how the magnitude of the frequency component in (Eq. 5.1) at $k = 1$ and $v = \pm 3$ from the leakage flux signal varies under different loading conditions and different phase to phase turn fault severities.

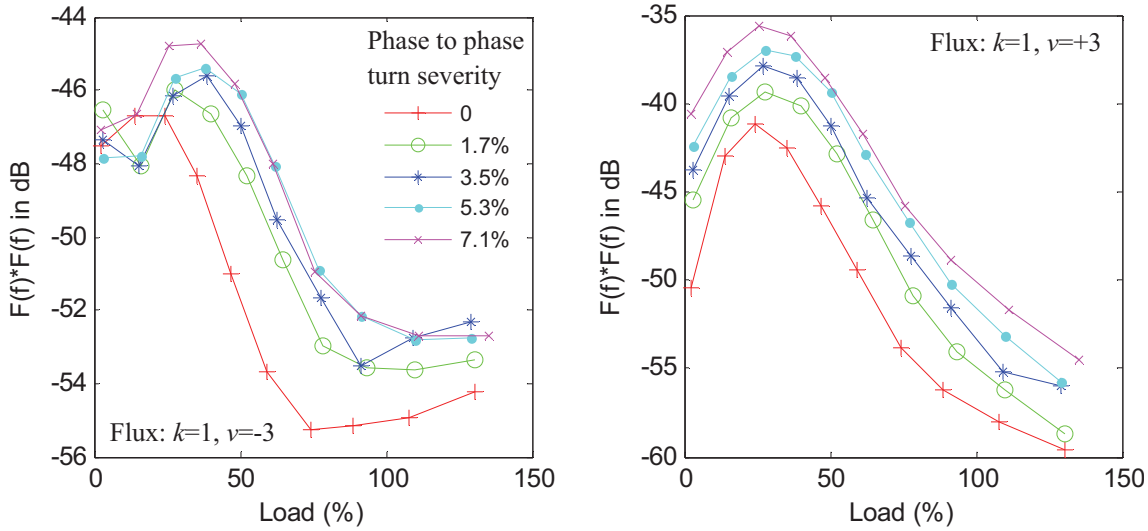

Figure A.15 - Magnitude of the frequency component in (Eq. 5.1) at $k = 1$ and $v = \pm 3$ from the leakage flux signal as a function of load.

A.8. Experimental Results for Phase to Phase Turn Fault Analysis Using Twice Supply Frequency

Figure A.16 and Figure A.17 show how the magnitude of the twice supply frequency component in the motor vibration signals varies under different loading conditions and different phase to phase turn fault severities.

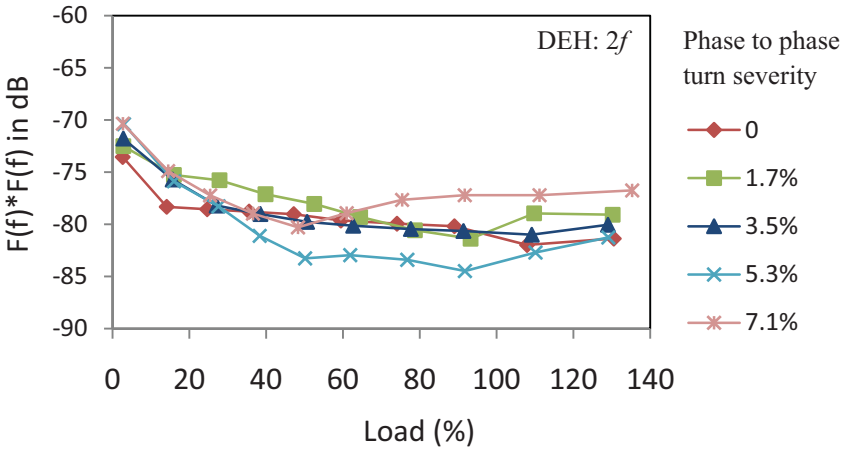

Figure A.16 - Magnitude of the twice supply frequency in the DEH vibration signal as a function of load.

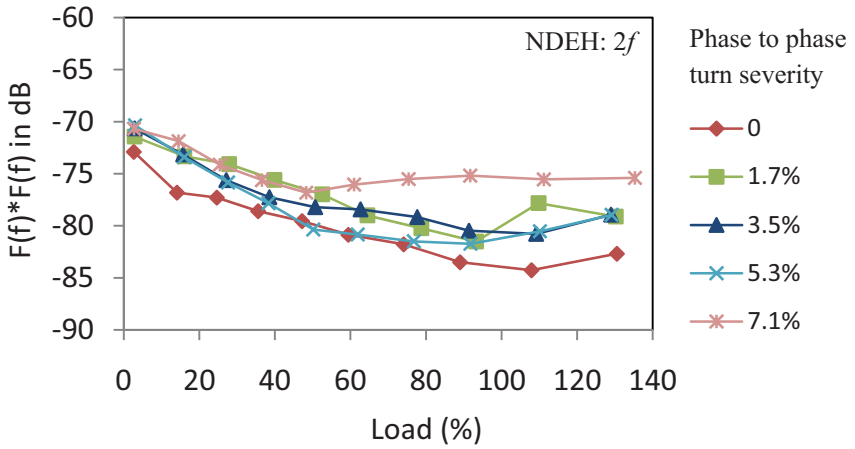

Figure A.17 - Magnitude of the twice supply frequency in the NDEH vibration signal as a function of load.

A.9. Experimental Results for Phase to Phase Turn Fault Analysis Using Rotor Slot Harmonics

Figure A.18 and Figure A.19 show how the magnitude of the frequency component in (Eq. 5.3) at $n_d = 0$, $k = 1$ and $v = \pm 1, \pm 3$ from the leakage flux signal varies as functions of loading condition and phase to phase turn fault severity.

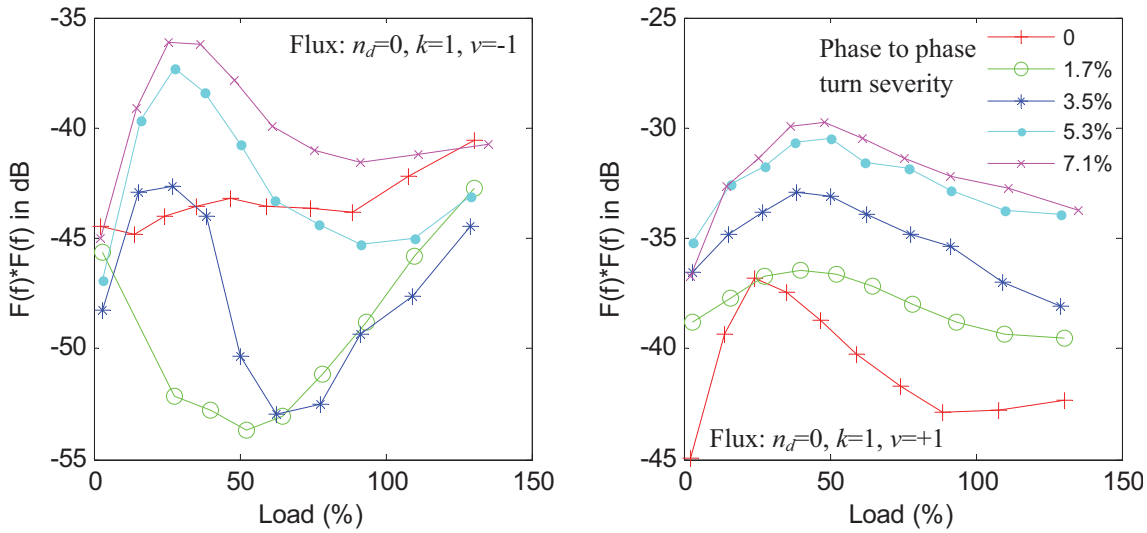

Figure A.18 - Magnitude of the frequency component in (Eq. 5.3) at $n_d = 0$, $k = 1$ and $v = \pm 1$ from the leakage flux signal as a function of load.

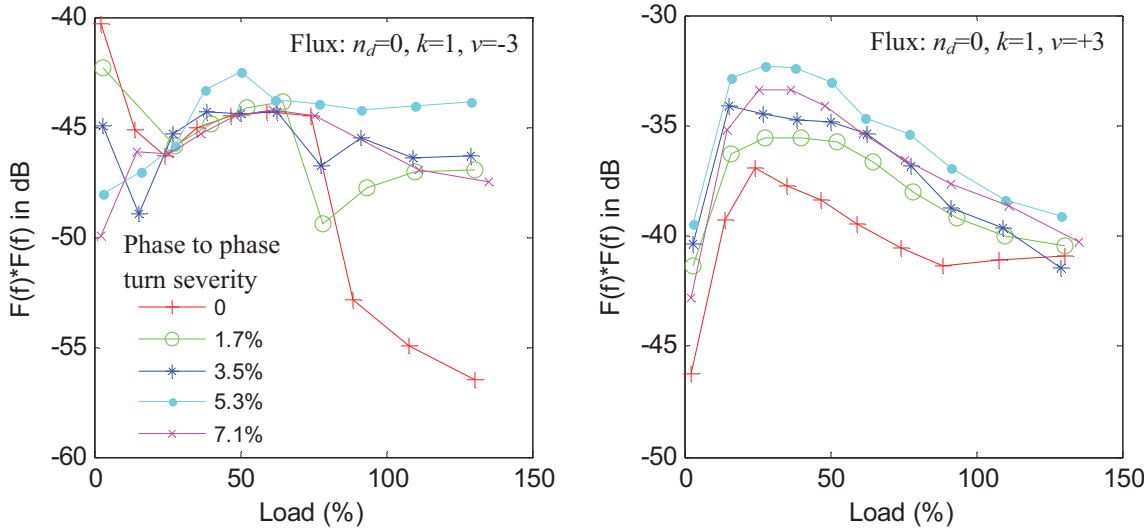

Figure A.19 - Magnitude of the frequency component in (Eq. 5.3) at $n_d = 0$, $k = 1$ and $v = \pm 3$ from the leakage flux signal as a function of load.

A.10. Experimental Results for Phase to Phase Turn Fault Analysis Using Third Harmonic of the Fundamental

Figure A.20 and Figure A.21 show how the magnitude of the frequency component at $3f$ in the stator current and the leakage flux signals varies as functions of loading condition and phase to phase turn fault severity.

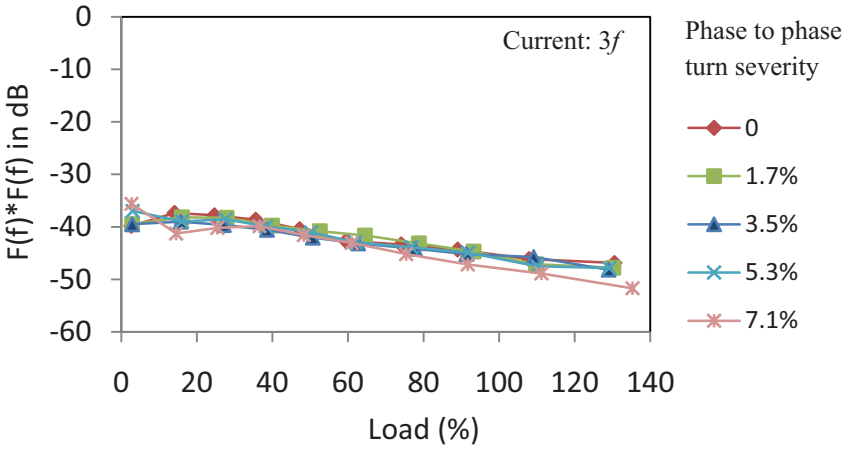

Figure A.20 - Magnitude of the third supply harmonic in the current signal as a function of load.

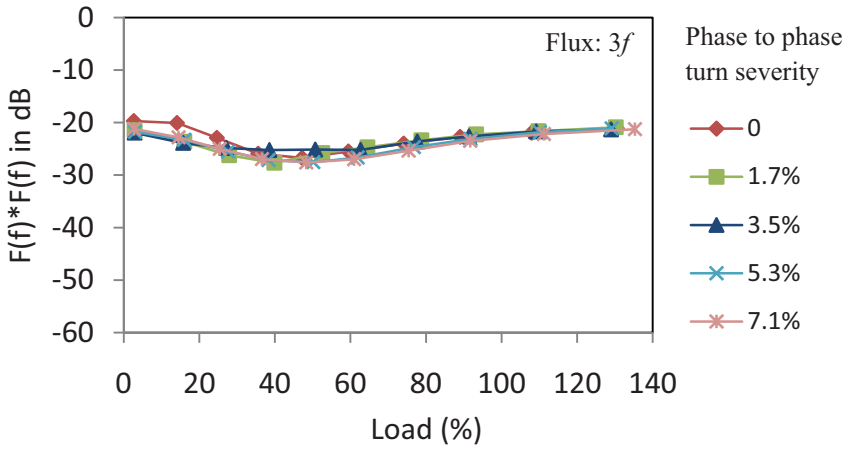

Figure A.21 - Magnitude of the third supply harmonic in the leakage flux signal as a function of load.

Appendix B. Further Results of the Static Eccentricity Fault Test

B.1. Experimental Results for Static Eccentricity Fault Analysis Using Rotor Slot Harmonics

Figure B.1 and Figure B.2 show how the magnitude of the dynamic eccentricity components of the rotor slot harmonics in (Eq. 6.1) from the stator current and axial leakage flux signals varies under different loading conditions and different static eccentricity severities.

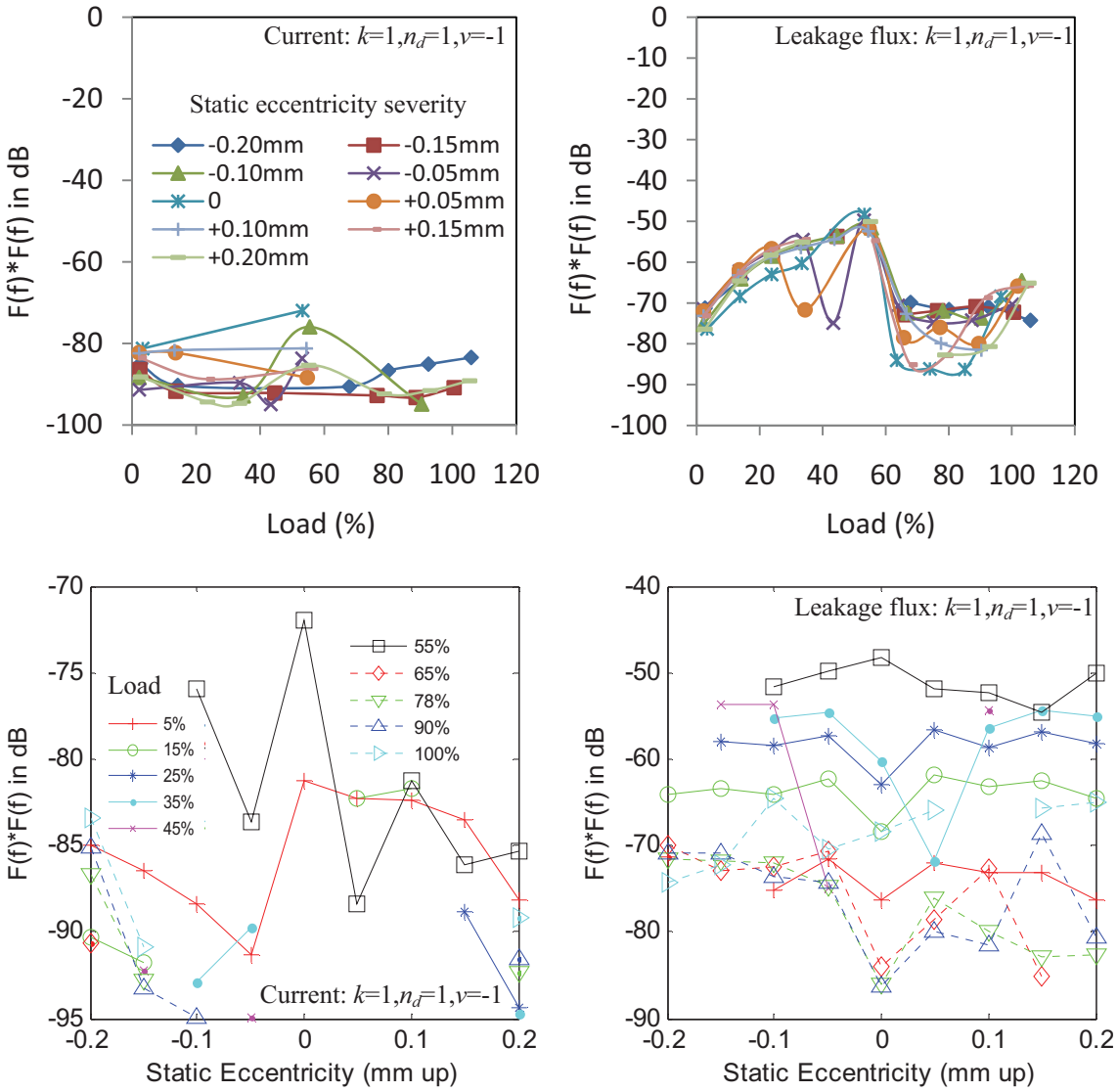

Figure B.1 – Magnitude of the lower sideband of the dynamic eccentricity components in (Eq. 6.1) from the current and the leakage flux signals as a function of load (top) and as a function of static eccentricity level (bottom).

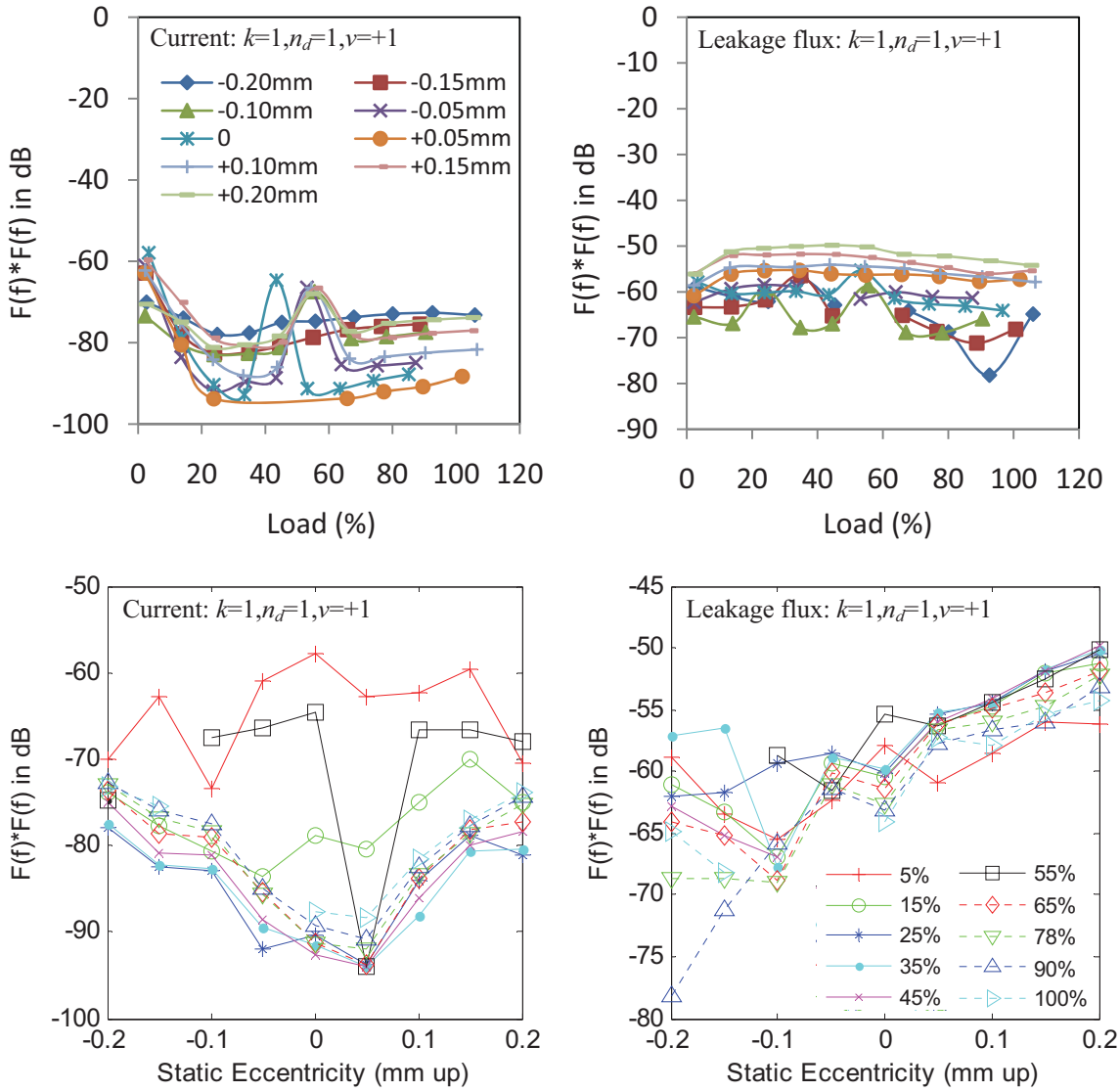

Figure B.2 – Magnitude of the upper sideband of the dynamic eccentricity components in (Eq. 6.1) from the current and the leakage flux signals as a function of load (top) and as a function of static eccentricity level (bottom).

B.2. Experimental Results for Static Eccentricity Fault Analysis Using Rotor Frequency Sidebands of the Fundamental

Figure B.3 and Figure B.4 show how the magnitude of the frequency components in (Eq. 6.2) from the current and leakage flux signals varies under different loading conditions and different static eccentricity severities.

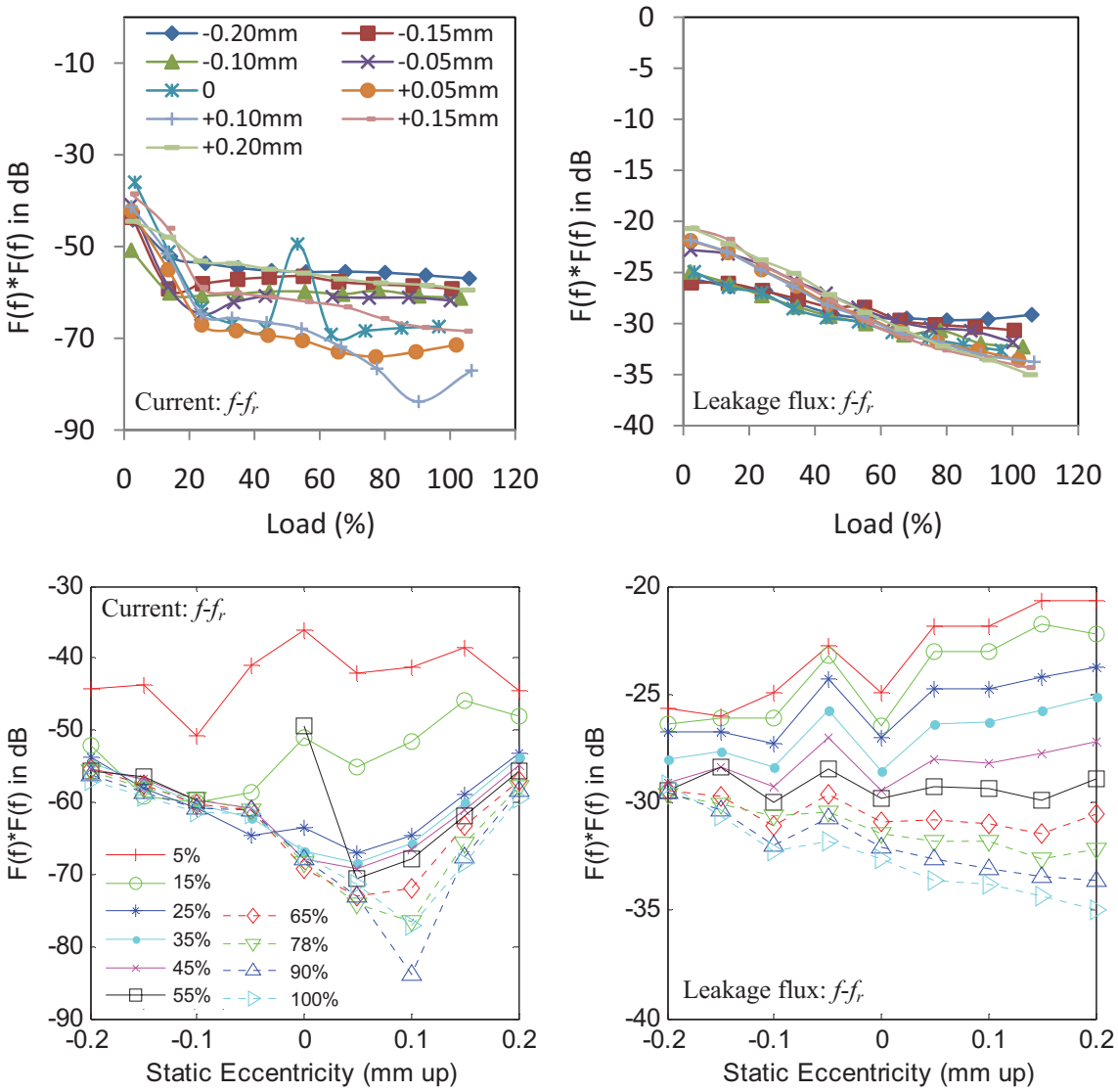

Figure B.3 – Magnitude of the lower sideband of the frequency components in (Eq. 6.2) from the current and the leakage flux signals as a function of load (top) and as a function of static eccentricity level (bottom).

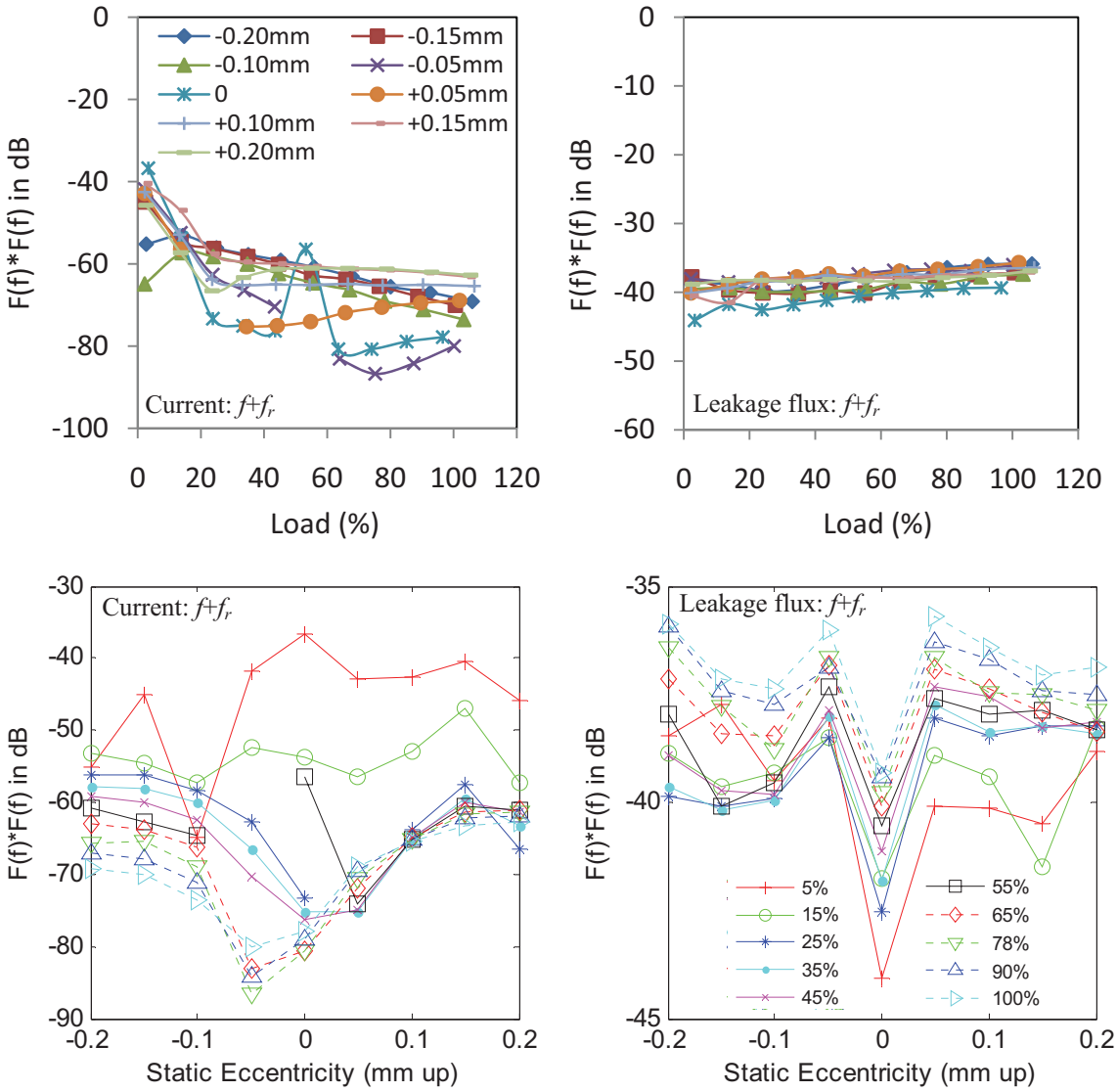

Figure B.4 – Magnitude of the upper sideband of the frequency components in (Eq. 6.2) from the current and the leakage flux signals as a function of load (top) and as a function of static eccentricity level (bottom).

B.3. Experimental Results for Static Eccentricity Fault Analysis Using Rotor Frequency Sidebands of Twice the Fundamental

Figure B.5 shows how the magnitude of the frequency components in (Eq. 6.3) from the motor vibration signal varies under different loading conditions and different static eccentricity severities.

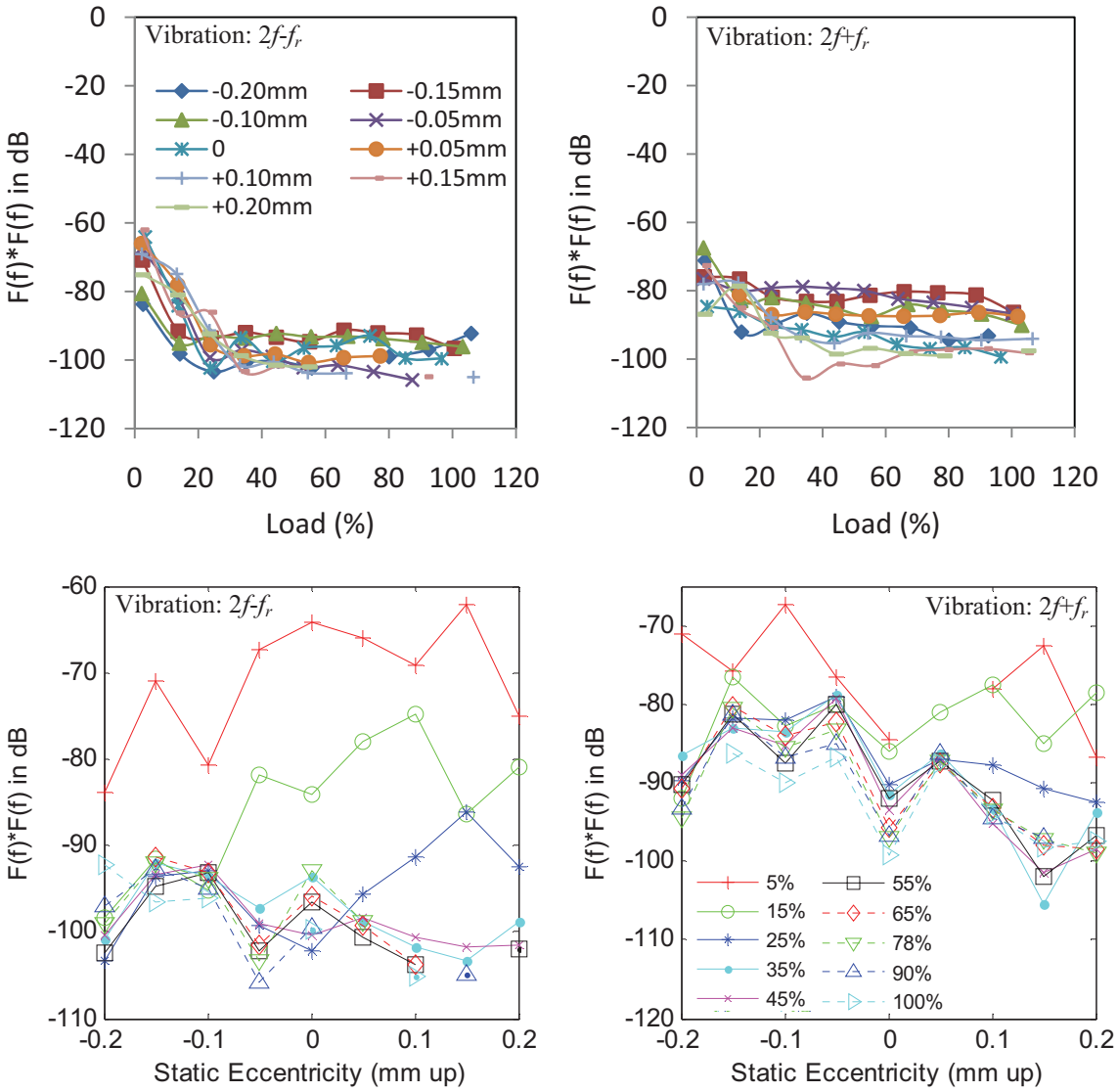

Figure B.5 – Magnitude of the rotor frequency sidebands of the twice fundamental (Eq. 6.3) from the vibration signal as a function of load (top) and as a function of static eccentricity level (bottom).

B.4. Experimental Results for Static Eccentricity Fault Analysis Using Third Harmonic of Rotor Frequency

Figure B.6 shows how the magnitude of the frequency component at $3f_r$ in the motor vibration signal varies under different loading conditions and different static eccentricity severities.

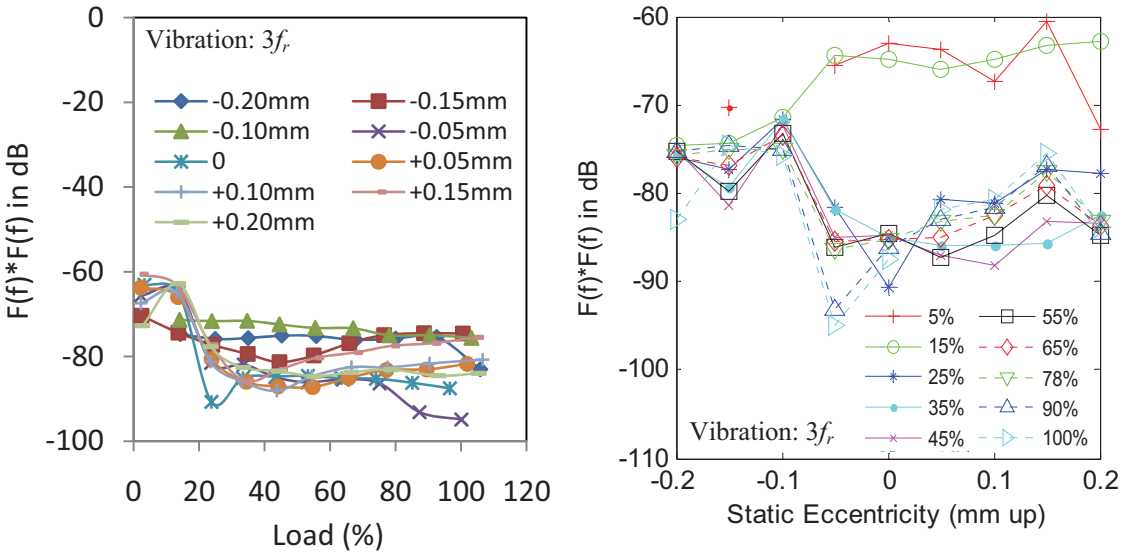

Figure B.6 – Magnitude of the third harmonic of the rotor frequency (Eq. 6.4) from the vibration signal as a function of load (left) and as a function of static eccentricity level (right).

B.5. Experimental Results for Static Eccentricity Fault Analysis Using Twice Supply Frequency

Figure B.7 shows how the magnitude of the frequency component at $2f$ in the motor vibration signal varies under different loading conditions and different static eccentricity severities.

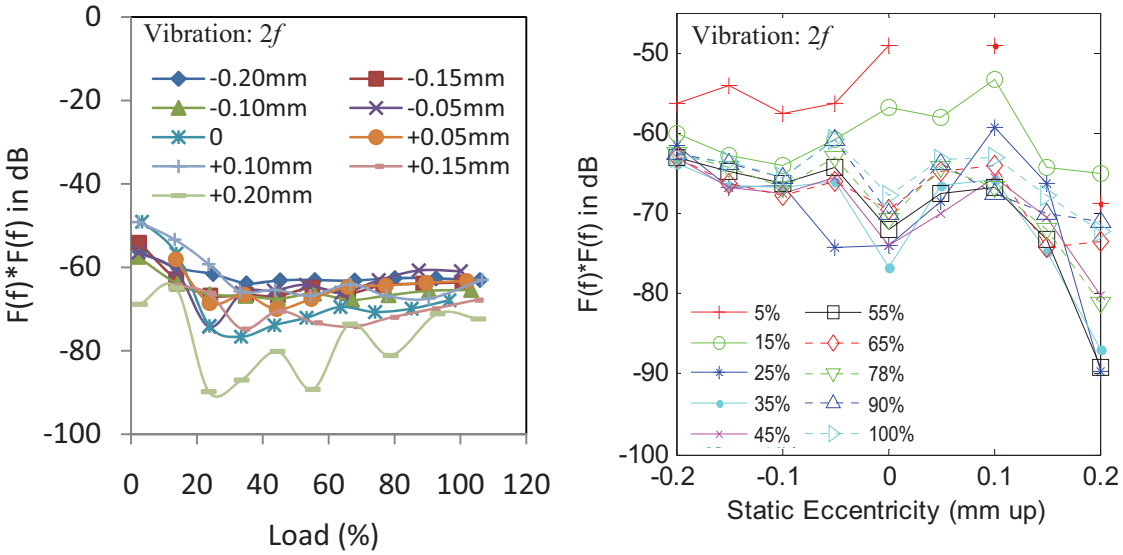

Figure B.7 – Magnitude of the twice supply frequency (Eq. 6.5) in the vibration signal as a function of load (left) and as a function of static eccentricity level (right).

B.6. Experimental Results for Static Eccentricity Fault Analysis Using Rotor Frequency

Figure B.8 shows how the magnitude of the frequency component at f_r in the motor vibration signal varies under different loading conditions and different static eccentricity severities.

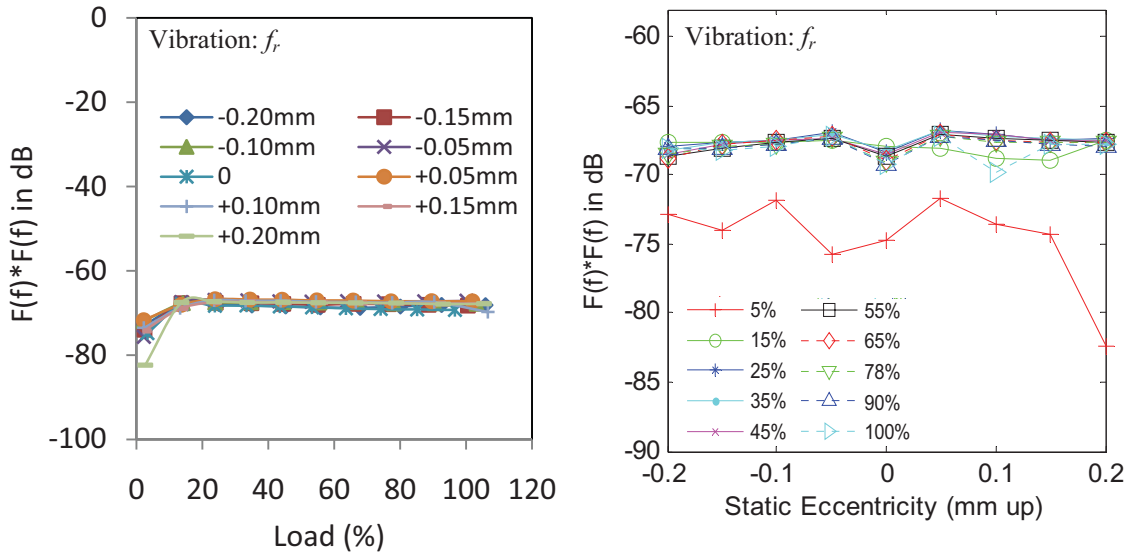

Figure B.8 – Magnitude of the rotor frequency (Eq. 6.6) in the vibration signal as a function of load (left) and as a function of static eccentricity level (right).

B.7. Experimental Results for Static Eccentricity Fault Analysis Using Second Harmonic of Rotor Frequency Sidebands of the Fundamental

Figure B.9 shows how the magnitude of the frequency components in (Eq. 6.7) from the motor vibration signal varies under different loading conditions and different static eccentricity severities.

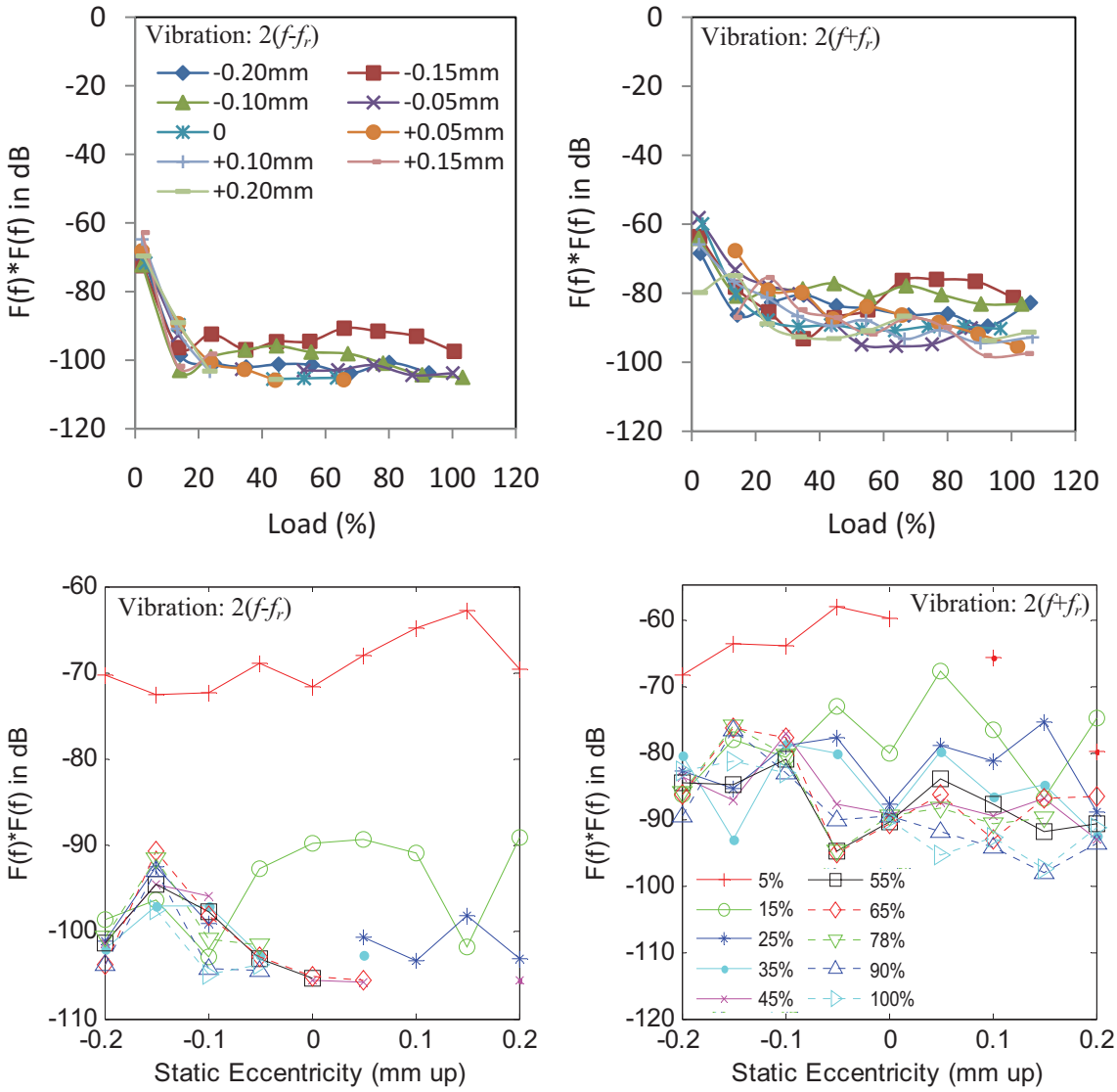

Figure B.9 – Magnitude of the second harmonic of the rotor frequency sidebands of the fundamental (Eq. 6.7) in the vibration signal as a function of load (top) and as a function of static eccentricity level (bottom).

B.8. Experimental Results for Static Eccentricity Fault Analysis Using RMS Vibration

Figure B.10 shows how the RMS vibration level varies under different loading conditions and different static eccentricity severities.

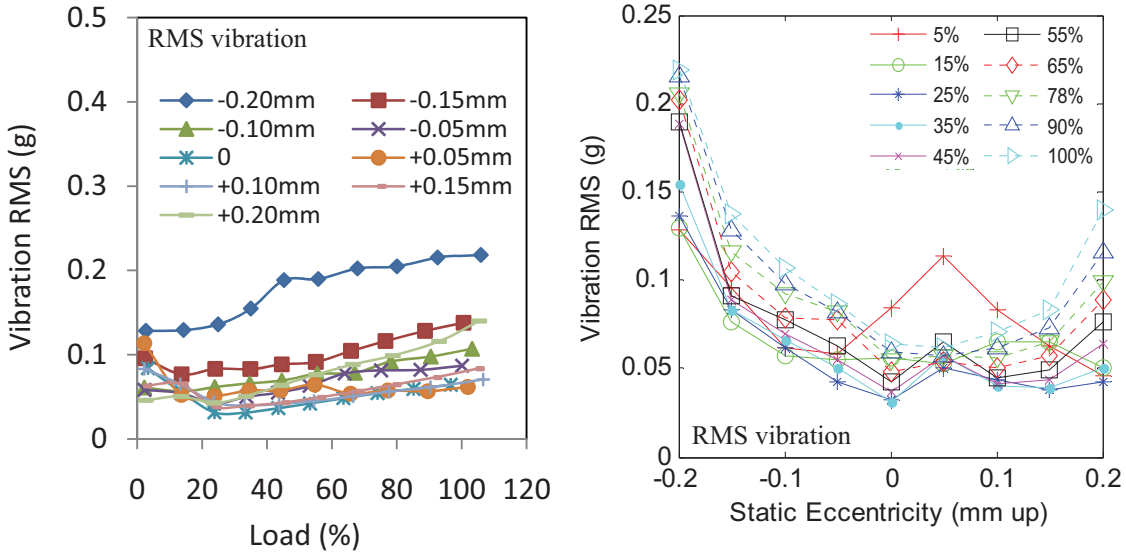

Figure B.10 – Magnitude of the RMS vibration as a function of load (left) and as a function of static eccentricity level (right).

Reference List

[1] H. W. Penrose, "Test Methods for Determining the Impact of Motor Condition on Motor Efficiency and Reliability," BJM Corp, ALL-TEST Division, Old Saybrook, CT 06475.

[2] W. T. Thomson and M. Fenger, "Current Signature Analysis to Detect Induction Motor Faults," *IEEE Industry Applications Magazine,* vol. 7, pp. 26-34, July-August 2001.

[3] M. E. H. Benbouzid, "A Review of Induction Motor Signature Analysis as a Medium for Faults Detection," *IEEE Transactions on Industrial Electronics,* vol. 47, pp. 984-993, October 2000.

[4] W. T. Thomson, "A Review of On-line Condition Monitoring Techniques for Three-Phase Squirrel Cage Induction Motors — Past Present and Future," in *IEEE SDEMPED*, Spain, 1999, pp. 3-18.

[5] M. M. O'Kane and M. J. Sander, "Intelligent Motors Move to the Forefront of Predictive Maintenance," in *IEEE Industry Applications Magazine*, 2000, pp. 47-51.

[6] N. Ertugrul, "Condition Monitoring: Power Quality and Condition Monitoring," University of Adelaide, School of Electrical and Electronic Engineering, Adelaide, Lecture Notes 27 April 2004.

[7] A. G. Innes, "Condition Monitoring of Induction Motors: The Detection of Broken Rotor Bars in Variable Speed Induction Motor Drives." vol. Doctor of Philosophy: University of Tasmania, 1999, p. 201.

[8] Y. Han and Y. H. Song, "Condition Monitoring Techniques for Electrical Equipment - A Literature Survey," *IEEE Transactions on Power Delivery,* vol. 18, January 2003.

[9] R. Fiser and S. Ferkolj, "Application of Finite Element Method to Predict Damaged Induction Motor Performance," *IEEE Transactions on Magnetics,* vol. 37, pp. 3635-3639, September 2001.

[10] M. Y. Chow, *Methodologies of Using Neural Network and Fuzzy Logic Technologies for Motor Incipient Fault Detection*. Singapore: World Scientific Publishing Co. Pte. Ltd., 1997.

[11] F. Filippetti, C. Tassoni, G. Franceschini, and P. Vas, "Integrated Condition Monitoring and Diagnosis of Electrical Machines Using Minimum Configuration Artificial Intelligence," in *European Power Electronics Conference*, 1997, pp. 2983-2988.

[12] F. Filippetti, M. Martelli, G. Franceschini, and C. Tassoni, "Development of Expert System Knowledge Base to On-line Diagnosis of Rotor Electrical Faults of Induction Motors," *Industry Applications Society Annual Meeting, Conference Record of the 1992 IEEE,* vol. 1, pp. 92-99, 1992.

[13] D. G. Dorrell, W. T. Thomson, and S. Roach, "Analysis of Airgap Flux, Current, and Vibration Signals as a Function of the Combination of Static and Dynamic Airgap Eccentricity in 3-Phase Induction Motors," *IEEE Transactions on Industry Applications,* vol. 33, pp. 24-34, January-February 1997.

[14] S. H. Kim, T. S. Park, J. Y. Yoo, and G. T. Park, "Speed-Sensorless Vector Control of an Induction Motor Using Neural Network Speed Estimation," *IEEE Transactions on Industrial Electronics,* vol. 48, pp. 609-614, June 2001.

[15] M. L. Sin, W. L. Soong, and N. Ertugrul, "Induction Machine On-Line Condition Monitoring and Fault Diagnosis - A Survey," in *AUPEC2003*, Christchurch, New Zealand, 2003.

[16] O. V. Thorsen and M. Dalva, "Failure Identification and Analysis for High-Voltage Induction Motors in the Petrochemical Industry," *IEEE Transactions on Industry Applications,* vol. 35, pp. 810-818, July - August 1999.

[17] IAS Motor Reliability Working Group, "Report of Large Motor Reliability Survey of Industrial and Commercial Installations - Part I," *IEEE Transactions on Industry Applications,* vol. 21, pp. 853-864, July-August 1985.

[18] J. Siau, A. Graff, W. L. Soong, and N. Ertugrul, "Broken Bar Detection in Induction Motors Using Current and Flux Spectral Analysis," *Australian Journal of Electrical and Electronic Engineering,* vol. 1, pp. 171-177, 2004.

[19] H. Henao, C. Demian, and G.-A. Capolino, "A Frequency-Domain Detection of Stator Winding Faults in Induction Machines Using an External Flux Sensor," *IEEE Transactions on Industry Applications,* vol. 39, pp. 1272-1279, September-October 2003.

[20] M. F. Cabanas, M. G. Melero, G. A. Orcajo, F. Rodriguez Faya, and J. Solares Sariego, "Experimental Application of Axial Leakage Flux to the Detection of Rotor Asymmetries, Mechanical Anomalies and Interturn Short-Circuits in Working Induction Motors," in *International Conference on Electrical Machines*, 1998, pp. 420-425.

[21] A. H. Bonnet and G. C. Soukup, "Cause and Analysis of Stator and Rotor Failures in Three-Phase Squireel-Cage Induction Motors," *IEEE Transactions on Industry Applications,* vol. 28, pp. 921-937, July-August 1992.

[22] I. Ahmed, R. Supangat, J. Grieger, N. Ertugrul, and W. L. Soong, "A Baseline Study for On-Line Condition Monitoring of Induction Machines," in *Australasian Universities Power Engineering Conference (AUPEC)*, Brisbane, Australia, 2004.

[23] G. B. Kliman, W. J. Premerlani, B. Yazici, R. A. Koegl, and J. Mazereeuw, "Sensorless, Online Motor Diagnostics," *IEEE Computer Applications in Power,* pp. 39-43, April 1997.

[24] G. Franceschini and C. Tassoni, "Time Harmonic Investigation of Flux Density in the Stator and Rotor Frame Oriented to Diagnosis of Cage Induction Machines," in *Electrical Machines and Drives*, Oxford, UK, 1993, pp. 103-108.

[25] J. R. Cameron, W. T. Thomson, and A. B. Dow, "Vibration and Current Monitoring for Detecting Airgap Eccentricity in Large Induction Motors," in *IEE Proceedings Pt. B*, 1986, pp. 155-163.

[26] C. Kral, T. G. Habetler, and R. G. Harley, "Detection of Mechanical Imbalances without Frequency Analysis," in *4th IEEE International Symposium on Diagnostics for Electric Machines, Power Electronics and Drives*, 2003, pp. 317 - 321.

[27] S. Nandi and H. A. Toliyat, "Condition Monitoring and Fault Diagnosis of Electrical Machines - A Review," *IEEE Industrial Applications Society Annual Meeting,* vol. 1, pp. 197-204, October 1999.

[28] R. R. Schoen and T. G. Habetler, "Effects of Time-Varying Loads on Rotor Fault Detection in Induction Machines," *IEEE Transactions on Industry Applications,* vol. 31, pp. 900-906, July-August 1995.

[29] W. T. Thomson, D. Rankin, and D. G. Dorrell, "On-Line Current Monitoring To Diagnose Airgap Eccentricity In Large Three-Phase Induction Motors - Industrial Case Histories Verify The Predictions," *IEEE Transactions on Energy Conversion,* vol. 14, pp. 1372-1378, December 1999.

[30] N. Arthur and J. Penman, "Induction Machine Condition Monitoring with Higher Order Spectra," *IEEE Transactions on Industrial Electronics,* vol. 47, October 2000.

[31] G. Stone and J. Kapler, "Stator Winding Monitoring," in *IEEE Industry Applications Magazine*. vol. 4, 1998, pp. 15-20.

[32] M. Arkan and P. Unsworth, "Online Stator Fault Diagnosis in Induction Motors," in *IEE Proceeding - Electrical Power Application*, 2001, pp. 537-547.

[33] W. T. Thomson, "On-line MCSA to Diagnose Shorted Turns in Low Voltage Stator Windings of 3-phase Induction Motors Prior to Failure," in *Electrical Machines and Drives Conference Proceeding*, Cambridge, MA, 2001, pp. 891-898.

[34] J. S. Kohler, J. Sottile, and F. C. Trutt, "Alternatives for Assessing the Electrical Integrity of Induction Motors," *IEEE Transactions on Industry Applications,* vol. 28, pp. 1109-1117, September-October 1992.

[35] J. S. Hsu, "Monitoring of Defects in Induction Motors through Air-gap Torque Observation," *IEEE Transactions on Industry Applications,* vol. 31, pp. 1016-1021, September-October 1995.

[36] G. M. Joksimovic and J. Penman, "The Detection of Inter-Turn Short Circuits in the Stator Windings of Operating Motors," *IEEE Transactions on Industrial Electronics,* vol. 47, October 2000.

[37] A. Stavrou, H. G. Sedding, and J. Penman, "Current Monitoring for Detecting Inter-Turn Short Circuits in Induction Motors," *IEEE Transactions on Energy Conversion,* vol. 16, March 2001.

[38] B. Martin, "Mechanical Signature Analysis," University of Adelaide, Adelaide, School of Mechanical Engineering Lecture Notes 2003.

[39] J. F. Watson and N. C. Paterson, "Improved Techniques for Rotor Fault Detection in Three-Phase Induction Motors," in *IEEE Industry Applications Conference Part 1 (of 3)*, St.Louis, MO, USA, 1998, pp. 271-277.
[40] E. Kreyszig, *Advanced Engineering Mathematics*, 8 ed. Ohio, Columbus: John Wiley & Sons, Inc., 1998.
[41] A. Ambardar, *Analog and Digital Signal Processing*, 2 ed. USA: Brooks-Cole ITP, 1999.
[42] C. E. Shannon and W. Weaver, *The Mathematical Theory of Communication*. Urbana USA: University of Illinois Press, 1971.
[43] C. S. Burrus and T. W. Parks, *DFT/FFT and Convolution Algorithms: Theory and Implementation*. New York: John Wiley & Sons, 1985.
[44] F. J. Harris, "On The Use of Windows for Harmonic Analysis with The Discrete Fourier Transform," in *IEEE*, 1978, pp. 51-83.
[45] A. H. Nuttall, "Some Windows with Very Good Sidelobe Behaviour," *IEEE Transactions on Acoustics, Speech and Signal Processing,* vol. 29, pp. 84-91, February 1981.
[46] G. Carlson, *Signal and Linear Analysis*, 2 ed.: Wiley & Sons, 1998.
[47] J. C. Goswami and A. K. Chan, *Fundamentals of Wavelets: Theory, Algorithms, and Applications*: Wiley, 1999.
[48] H. K. Chul and R. Aggarwal, "Wavelet Transforms in Power Systems. II. Examples of Application to Actual Power System Transients," *Power Engineering Journal,* vol. 15, pp. 193-202, August 2001.
[49] I. Daubechies, "The wavelet transform, time-frequency localization and signal analysis," *IEEE Transactions on Information Theory,* vol. 36, pp. 961-1005, 1990.
[50] A. M. Gargoom, "Digital Signal Processing Techniques for Improving the Automatic Classification of Power Quality Events," in *Electrical and Electronic Engineering*. vol. Doctor of Philosophy Adelaide, Australia: University of Adelaide, 2006.
[51] P. Pillay and A. Bhattacharjee, "Application of Wavelets to Model Short-Term Power System Disturbances," *IEEE Transactions on Power Systems,* vol. 11, pp. 2031-2037, November 1996.
[52] Y. T. Chan, *Wavelet Basics*, 1 ed.: Springer, 1995.
[53] M. Xu, "Orders Tracking Analysis of Variable Speed Machines," in *Enteract International: Information Through Integration*, Cincinnati, Ohio, 1998.
[54] K. R. Fyfe and E. D. S. Munck, "Analysis of Computed Order Tracking," *Mechanical Systems and Signal Processing,* vol. 11, pp. 187-205, 1997.
[55] R. Blasco, M. Sumner, and G. M. Asher, "Speed Measurement of Inverter Fed Induction Motors Using the FFT and the Rotor Slot Harmonics," in *Power Electronics and Variable-Speed Drives*, London, 1994, pp. 470-475.
[56] A. Ferrah, K. G. Bradley, and G. M. Asher, "Sensorless Speed Detection of Inverter Fed Induction Motors using Rotor Slot Harmonics and Fast Fourier Transform," in *Power Electronics Specialists Conference*, Toledo, 1992, pp. 279-286.
[57] K. D. Hurst and T. G. Habetler, "Sensorless Speed Measurement Using Current Harmonic Spectral Estimation in Induction Machine Drives," *IEEE Transactions on Power Electronics,* vol. 11, pp. 66-73, January 1996.
[58] K. D. Hurst and T. G. Habetler, "A Comparison of Spectrum Estimation Techniques for Sensorless Speed Detection in Induction Machines," *IEEE Transactions on Industry Applications,* vol. 33, pp. 898-905, July-August 1997.

[59] R. B. Blackman and J. W. Tukey, *The Measurement of Power Spectra*. New York: Dover, 1958.
[60] K. Steiglitz and L. McBride, "A Technique for the Identification of Linear Systems," *IEEE Transactions on Automatic Control,* vol. 10, pp. 461-464, October 1965.
[61] R. D. Schmidt, "Multiple Emitter Location and Signal Parameter Estimation," *IEEE Transactions on Antennas and Propagation,* vol. 34, pp. 276-280, March 1986.
[62] D. Shi, P. J. Unsworth, and R. X. Gao, "Sensorless Speed Measurement of Induction Motor Using Hilbert Transform and Interpolated Fast Fourier Transform," *IEEE Transactions on Instrumentation and Measurement,* vol. 55, pp. 290-299, February 2006.
[63] K. L. Shi, T. F. Chan, Y. K. Wong, and S. L. Ho, "Speed Estimation of an Induction Motor Drive Using an Optimized Extended Kalman Filter," *IEEE Transactions on Industrial Electronics,* vol. 49, pp. 124-133, February 2002.
[64] B. Kaku, I. Miyashita, and S. Yasukawa, "Novel Speed Estimation Method for Induction Motor Based on Extra Rotor Synchronous Current Control," in *IEEE Power Electronics Specialists Conference*, Fukuoka, 1998, pp. 852-856.
[65] A. Consoli, G. Scarcella, and A. Testa, "On the Use of Sensorless Induction Motor Drives as Speed Sensors," in *IEEE Industrial Electronics Society (IECON)*, 2003, pp. 1472-1478.
[66] J. Penman, H. G. Sedding, B. A. Lloyd, and W. T. Fink, "Detection and Location of Interturn Short Circuits in the Stator Windings of Operating Motors," *IEEE Transactions on Energy Conversion,* vol. 9, pp. 652-658, 1994.
[67] S. M. A. Cruz and A. J. M. Cardoso, "Diagnosis of Stator Inter-Turn Short Circuits in DTC Induction Motor Drives," *IEEE Transactions on Industry Applications,* vol. 40, pp. 1349-1360, September-October 2004.
[68] H. Nejjari and M. E. H. Benbouzid, "Monitoring and Diagnosis of Induction Motors Electrical Faults Using a Current Park's Vector Pattern Learning Approach," *IEEE Transactions on Industry Applications,* vol. 36, May-June 2000.
[69] S. M. A. Cruz and A. J. M. Cardoso, "Stator Winding Fault Diagnosis in Three-Phase Synchronous and Asynchronous Motors, by the Extended Park's Vector Approach," *IEEE Transactions on Industry Applications,* vol. 37, pp. 1227-1233, September-October 2001.
[70] S. M. A. Cruz and A. J. M. Cardoso, "Rotor Cage Fault Diagnosis in Three-Phase Induction Motors by Extended Park's Vector Approach," *Electrical Machines and Power Systems,* vol. 28, pp. 289-299, 2000.
[71] F. Filippetti, G. Franceschini, G. Gentile, S. Meo, A. Ometto, N. Rotondale, and C. Tassoni, "Deterministic Approach and Neural Network Approach for Stator Short Circuits Diagnosis in Induction Machines," in *EPE Conference Proceeding*, Trondheim, Norway, 1997.
[72] G. B. Kliman, W. J. Premerlani, R. A. Koegl, and D. Hoeweler, "Sensitive, On-Line Turn-to-Turn Fault Detection in AC Motors," *Electric Power Components and Systems,* vol. 28, pp. 915-927, October 2000.
[73] R. M. Tallam, T. G. Habetler, R. G. Harley, D. J. Gritter, and B. H. Burton, "Neural Network based On-line Stator Winding Turn Fault Detection for Induction Motors," in *IEEE Industry Applications Conference*. vol. 1, 2000, pp. 375-380.

[74] M. Haji and H. A. Toliyat, "Pattern Recognition - A Technique for Induction Machines Rotor Fault Detection "Eccentricity And Broken Bar Fault"," in *Thirty-Sixth IAS Annual Meeting*, Chicago, IL, 2001, pp. 1572-1578.
[75] S. E. Zocholl, "Introduction to Symmetrical Components," Schweitzer Engineering Laboratories, Inc., Pullman, WA 2004.
[76] S. Nandi, S. Ahmed, and H. A. Toliyat, "Detection of Rotor Slot and Other Eccentricity Related Harmonics in a Three Phase Induction Motor with Different Rotor Cages," *IEEE Transactions on Energy Conversion,* vol. 16, pp. 253-260, September 2001.
[77] H. A. Toliyat, M. S. Arefeen, and A. G. Parlos, "A Method for Dynamic Simulation and Detection of Air-gap Eccentricity in Induction Machines," in *Thirtieth IAS Annual Meeting*, Orlando, FL, 1995, pp. 629-636.
[78] W. T. Thomson and A. Barbour, "The On-Line Prediction Of Airgap Eccentricity Levels In Large (MW Range) 3-Phase Induction Motors," in *International Conference IEMD*, 1999.
[79] S. Nandi, R. M. Bharadwaj, and H. A. Toliyat, "Performance Analysis of a Three-Phase Induction Motor Under Mixed Eccentricity Condition," *IEEE Transactions on Energy Conversion,* vol. 17, 2002.
[80] S. M. A. Cruz, A. J. M. Cardoso, and H. A. Toliyat, "Diagnosis of Stator, Rotor and Airgap Eccentricity Faults in Three-Phase Induction Motors Based on the Multiple Reference Frames Theory," in *38th IAS Annual Meeting*, 2003.
[81] A. J. M. Cardoso and E. S. Saraiva, "Predicting the Level of Airgap Eccentricity in Operating Three-Phase Induction Motors, by Park's Vector Approach," in *Industry Applications Society Annual Meeting*, Houston, TX, 1992, pp. 132-135.
[82] W. T. Thomson and A. Barbour, "On-line Current Monitoring and Application of a Finite Element Method to Predict the Level of Static Airgap Eccentricity in Three-Phase Induction Motors," *IEEE Transactions on Energy Conversion,* vol. 13, pp. 347-357, December 1998.
[83] S. Nandi, S. Ahmed, H. A. Toliyat, and R. M. Bharadwaj, "Selection Criteria of Induction Machines for Speed-Sensorless Drive Applications," *IEEE Transactions on Industry Applications,* vol. 39, pp. 704-712, May-June 2003.
[84] R. R. Obaid, T. G. Habetler, and R. M. Tallam, "Detecting Load Unbalance and Shaft Misalignment using Stator Current in Inverter-Driven Induction Motors," in *Electric Machines and Drives Conference, IEMDC'03*, 2003, pp. 1454-1458.
[85] A. Bellini, F. Filippetti, G. Franceschini, C. Tassoni, and G. B. Kliman, "Quantitative Evaluation of Induction Motor Broken Bars by Means of Electrical Signature Analysis," *IEEE Transactions on Industry Applications,* vol. 37, pp. 1248-55, 2001.
[86] S. M. Kay and S. L. Marple, Jr., "Spectrum Analysis - A Modern Perspective," in *IEEE Proceedings*, 1981, pp. 1380-1417.
[87] H. Douglas, P. Pillay, and A. K. Ziarani, "A New Algorithm for Transient Motor Current Signature Analysis Using Wavelets," *IEEE Transactions on Industry Applications,* vol. 40, pp. 1361-1368, September-October 2004.
[88] Z. Zhang, Z. Ren, and W. Huang, "A Novel Detection Method of Motor Broken Rotor Bars based on Wavelet Ridge," *IEEE Transactions on Energy Conversion,* vol. 18, pp. 417-423, 2003.
[89] R. Burnett, J. F. Watson, and S. Elder, "The Application of Modern Signal Processing Techniques to Rotor Fault Detection and Location within Three Phase

Induction Motors," in *IEEE Instrumentation and Measurement Technology Conference*, Naltham, MA, USA, 1995, pp. 426-431.

[90] H. A. Toliyat and T. A. Lipo, "Transient Analysis of Cage Induction Machines under Stator, Rotor Bar and End Ring Faults," *IEEE Transactions on Energy Conversion,* vol. 10, pp. 241-247, 1995.

[91] F. Cupertino, E. de Vanna, L. Salvatore, and S. Stasi, "Comparison of Spectral Estimation Techniques Applied to Induction Motor Broken Bars Detection," in *Diagnostics for Electric Machines, Power Electronics and Drives (SDEMPED)*, Atlanta, GA, USA, 2003, pp. 129-134.

[92] H. Ma, "Analysis of Starting Performance of Induction Machines Under Rotor Winding Faults," in *Universities Power Engineering Conference (UPEC)*, 2004, pp. 555-558.

[93] P. Cooke, *Noise and Modulation in Communication Electronics*. Adelaide: P. Cooke, 2002.

[94] A. v. Jouanne and B. Banerjee, "Assessment of Voltage Unbalance," *IEEE Transactions on Power Delivery,* vol. 16, pp. 782-790, October 2001.

[95] F. Cupertino, E. de Vanna, L. Salvatore, and S. Stasi, "Analysis Techniques for Detection of IM Broken Rotor Bars After Supply Disconnection," *IEEE Transactions on Industry Applications,* vol. 40, March-April 2004.

[96] J. Milimonfared, H. M. Kelk, S. Nandi, A. D. Minassians, and H. A. Toliyat, "A Novel Approach for Broken Rotor Bar Detection in Cage Induction Motors," *IEEE Transactions on Industry Applications,* vol. 35, pp. 1000-1006, September-October 1999.

[97] S. H. Kia, H. Henao, G. A. Capolino, and C. Martis, "Induction Machine Broken Bars Fault Detection Using Stray Flux after Supply Disconnection," in *IECON*, Paris, France, 2006.

[98] J. R. Blough, D. L. Brown, and H. Vold, "The Time Variant Discrete Fourier Transform as an Order Tracking Method," *Society of Automotive Engineers (SAE),* 1997.

[99] M. Cirrincione, M. Pucci, G. Cirrincione, and G. A. Capolino, "A New Adaptive Integration Methodology for Estimating Flux in Induction Machine Drives," *IEEE Transactions on Power Electronics,* vol. 19, pp. 25-34, January 2004.